J. Fluid Mech. (2012), *vol.* 710, *pp.* 72–101.
doi:10.1017/jfm.2012.352

Bubble breakup simulation in nozzle flows

Oleg E. Ivashnyov and Marina N. Ivashneva†

Department of Gas and Wave Dynamics, Faculty of Mechanics and Mathematics,
Moscow MV Lomonosov State University, Moscow 119899, Russia

(Received 21 August 2011; revised 6 May 2012; accepted 4 July 2012;
first published online 23 August 2012)

Experiments on high-pressure vessel decompression have shown that vaporization occurs in 'boiling shocks' moving with a velocity of $\sim$10 m s^{-1}. To explain this phenomenon, a model accounting for bubble breakup was suggested (Ivashnyov, Ivashneva & Smirnov, *J. Fluid. Mech.*, vol. 413, 2000, pp. 149–180). It was shown that the explosive boiling was caused by chain bubble fragmentation, which led to a sharp increase in the interface area and instantaneous transformation of the mixture into an equilibrium state. In the present study, this model is used to simulate nozzle flows with no change in the free parameters chosen earlier for modelling a tube decompression. It is shown that an advanced model ensures the best correspondence to experiments for flashing flows in comparison with an equilibrium model and with a model of boiling at a constant number of centres. It is also shown that the formation of a boiling shock in a critical nozzle flow leads to autovibrations.

Key words: boiling, breakup, shock waves

1. Introduction

The subject of this study is high-speed boiling liquid fluxes (flashing flows) realized at specific flow rates $j \geqslant 2000$ kg m^{-2} s^{-1}, which are characterized by a strong intensity of phase transitions. Flashing flows can appear after damage to water-cooled nuclear reactors. The reactor cooling system includes channels of different geometry: tubes, leak limiters (Laval nozzles), throttles and so on. Distinct from models for a one-phase flow, which do not require any change in the free parameter that 'depends' on the channel geometry (viscosity coefficient in the model of a viscid fluid, and adiabatic exponent in the model of an ideal gas), flashing flow models need such a change. For example, the number of boiling centres, the free parameter of the model of Nigmatulin & Soplenkov (1980), is chosen as 0.5×10^9 m^{-3} to simulate high-pressure tube depressurization and is taken to be three orders of magnitude greater for a nozzle flow though the liquid is the same and its parameters are close (Nigmatulin 1991, p. II).

The aim of the present study is to simulate a nozzle flow with no change in the model's free parameters chosen to model a tube decompression. In Ivashnyov, Ivashneva & Smirnov (2000), experiments on tube decompression (Edwards & O'Brien 1970) were simulated with three models: an equilibrium one (Ivandaev & Gubaidullin 1978), a model of boiling at a constant number of centres (Nigmatulin & Soplenkov 1980) and a model accounting for bubble fragmentation (Ivashnyov *et al.*

† Email address for correspondence: ivashneva-m@mail.ru

2000). In the present study, the same models without change in their free parameters are applied to simulate nozzle flows.

1.1. *Brief analysis of models for flashing flow*

In an *equilibrium model*, the temperatures, pressures and velocities of the liquid and vapour phases are considered equal. The equilibrium model includes the equations of conservation for mixture mass, momentum and energy:

$$\frac{\partial(\rho F)}{\partial t} + \frac{\partial(\rho u F)}{\partial x} = 0, \tag{1.1}$$

$$\frac{\partial(\rho u F)}{\partial t} + \frac{\partial(\rho u^2 F)}{\partial x} + F\frac{\partial P}{\partial x} = -\xi\frac{\rho|u|}{2D}uF, \tag{1.2}$$

$$\frac{\partial\left[\rho F\left(i - \dfrac{P}{\rho} + \dfrac{u^2}{2}\right)\right]}{\partial t} + \frac{\partial\left[\rho u F\left(i + \dfrac{u^2}{2}\right)\right]}{\partial x} = 0, \tag{1.3}$$

$$\rho = (1-\alpha)\rho_l + \alpha\rho_g, \quad i = (1-\chi)i_l + \chi i_g, \quad \chi = \frac{\rho_g\alpha}{\rho}, \tag{1.4}$$

where ρ, ρ_l and ρ_g are the mixture, liquid and vapour densities; α and χ are the volumetric and mass vapour contents; u is the flow velocity averaged over the cross-section; F and D are the cross-sectional area and diameter of the channel; P is the pressure in the mixture; i is the mixture enthalpy; i_l and i_g are the liquid and vapour enthalpies; and ξ is the coefficient of wall friction.

Because the equilibrium model assumes the interfacial surface to be infinitely large, the phases always stay in equilibrium. The model has no free parameters.

In the *model of boiling at constant number of bubbles* (Nigmatulin & Soplenkov 1980), the liquid is assumed to boil on nucleation centres that exist within it. The model considers the pressures and velocities in the liquid and vapour phases to be equal, but the temperatures are considered to be different. The vapour is assumed to be saturated, whereas the liquid can be superheated. For pressures smaller than the critical pressure, the vapour density is assumed to be much less that the liquid one, $\rho_g \ll \rho_l$.

The model consists of the equations of conservation for the mixture mass, momentum and internal energy (1.1)–(1.3) given above and the following equation for the vapour mass balance:

$$\frac{\partial(\rho_g\alpha F)}{\partial t} + \frac{\partial(\rho_g\alpha u F)}{\partial x} = JF, \tag{1.5}$$

where J is the specific intensity of evaporation in a unit mixture volume.

The intensity of evaporation depends on the specific area of the phase interface, and the model needs an interfacial area transport (IAT) equation. In general form, the IAT equation includes source and sink terms taking into account bubble breakup and coalescence, wall nucleation, bubble condensation and other effects (Ishii & Hibiki 2006). In the model assuming that the bubble number per unit mixture mass is constant, the IAT equation has the very simple form

$$\frac{\partial(nF)}{\partial t} + \frac{\partial(nuF)}{\partial x} = 0, \tag{1.6}$$

where n is the bubble number per unit volume of the mixture. Equations (1.1) and (1.6) yield

$$\frac{\partial}{\partial t}\left(\frac{n}{\rho}\right) = 0. \tag{1.7}$$

For the case when the nucleation centres per unit mixture mass are uniform, the equation in the partial derivative (1.6) reduces to

$$c = \frac{n}{\rho} = \text{const}. \tag{1.8}$$

The only free parameter of the model is the number of centres that nucleate boiling per mixture mass $c = n/\rho$.

For the *model accounting for bubble fragmentation* (Ivashnyov *et al.* 2000), all the assumptions except for that about the equalities of phase velocities, which is replaced by the assumption of the smallness of the phase slip $|u_g - u_l| \ll u_l$, are the same as for the model of boiling at a constant number of bubbles (Nigmatulin & Soplenkov 1980). The model also includes (1.1)–(1.6), but the IAT equation (1.6) has a source term taking into account the bubble fragmentation:

$$\frac{\partial(nF)}{\partial t} + \frac{\partial(nuF)}{\partial x} = \rho F \psi, \tag{1.9}$$

where ψ is the intensity of bubble breakup.

Bubble breakup is considered to be caused by Kelvin–Helmholtz instability of the surface of a bubble overstreaming by fluid. To calculate the intensity of bubble fragmentation, the model is supplemented with the equation of motion of an individual dispersed unit (Drew & Passman 1998).

$$(\rho_g + C_{vm}\rho_l)\frac{\mathrm{d}_g u_g}{\mathrm{d}t} = \rho_l \frac{\mathrm{D}u}{\mathrm{D}t} + C_{vm}\rho_l \frac{\mathrm{D}u}{\mathrm{D}t} - \frac{3}{a}C_{vm}\rho_l(u_g - u)\frac{\mathrm{d}_g a}{\mathrm{d}t} - S(u_g - u), \tag{1.10}$$

$$S = \frac{3}{2a}C_\mu \rho_l |u_g - u|, \quad \frac{\mathrm{D}}{\mathrm{D}t} = \frac{\partial}{\partial t} + u\frac{\partial}{\partial x}, \quad \frac{\mathrm{d}_g}{\mathrm{d}t} = \frac{\partial}{\partial t} + u_g\frac{\partial}{\partial x}, \tag{1.11}$$

where C_{vm} is the virtual mass coefficient, equal to $1/2$ for spherical bubbles; S is the drag force per unit velocity; C_μ is the drag coefficient; a is the bubble radius; $\mathrm{D}/\mathrm{D}t$ is the material derivative following the mixture (following the liquid, as $u \approx u_l$ according to the model assumption); and $\mathrm{d}_g/\mathrm{d}t$ is the material derivative following the units.

On the right-hand side of (1.10), the first term is the buoyancy force, the two next are the virtual mass force, and the last one is the bubble drag force. The third term characterizes the change in the virtual mass force due to the growth (collapse) of a bubble: the virtual mass of a growing bubble increases and it slows down, in contrast to a collapsing bubble, which loses a part of its virtual mass and accelerates (see appendix A in Ivashnyov *et al.* 2000). Equation (1.10) in general form applicable for a breaking bubble is given below.

The model has two free parameters: the initial number of boiling centres per unit mixture mass c_0; and the critical Weber number We^* characterizing the stability of the phase interface.

Of course, for the 'practical purpose' of critical mass flux prediction, flashing flow models can be used that do not consider the interfacial area transport and do not involve the IAT equation in partial derivatives (1.9). In the SIRINGUE model (Boivin 1979), the vapour is considered to be saturated but the liquid to be overheated. The

model includes (1.1)–(1.5); the specific intensity of evaporation, term J in (1.5), is determined using the relaxation ratio,

$$J = \rho \frac{\chi_e - \chi}{\theta}, \tag{1.12}$$

where χ_e is the mass vapour content in the mixture under the condition of its conversion to the equilibrium state; θ is the time of the conversion, which is determined using the formula obtained from the comparison of the model predictions with the experiments using the MOBY DISK device (Bauer, Houdauer & Sureau 1977) as

$$\theta = \frac{660\rho^{1.89}}{P^{0.505}\alpha^{0.95}}. \tag{1.13}$$

The model proposed by Skorek & Papadimitriou (1997) uses the same assumptions of a saturated vapour and superheated liquid and consists of (1.1)–(1.5). But instead of the IAT equation (1.9) and the equation for the phase slip (1.10), to close the system of conservation equations, empirical dependences are used that determine the intensity of evaporation and the phase slip from the flow parameters, i.e. the volumetric vapour content, phase densities and others:

$$J = [J'_B + J''_B](1-\alpha) + J''_D\alpha, \tag{1.14}$$

$$\left.\begin{aligned} J'_B &= 24\left(\frac{3}{4}\pi\alpha\right)^{1/3} n_B^{2/3}\rho_l c_l \frac{\lambda_l}{\rho_g h^2}(T_l - T_s)^2, \\ J''_B &= \frac{2}{h}\sqrt{6\rho_l c_l \lambda_l |u_g - u_l| n_B \alpha}(T_l - T_s), \end{aligned}\right\} \tag{1.15}$$

$$J''_D = \frac{2}{h}\sqrt{6\rho_g c_g \lambda_g |u_g - u_l| n_D(1-\alpha)}(T_l - T_s), \tag{1.16}$$

where J'_B is the specific intensity of evaporation due to thermal conduction; J''_B is the intensity of evaporation due to bubble streamline; J''_D is the specific intensity of evaporation for translating droplets; n_B and n_D are bubble and droplet numbers per unit mixture volume, free model parameters; c_l and c_g are the isobaric specific heat for liquid and vapour phases; λ_l and λ_g are the coefficients for thermal liquid and vapour conductivity; h is the specific heat of vaporization; and T_l and T_s are the liquid and vapour temperatures (according to the model assumption, the vapour temperature is equal to the saturation temperature, $T_s = T_s(P) = T_g$.

Phase velocities are determined using the dependence obtained from the handling of the experiments on critical flows of Henry (1968):

$$\frac{u_g}{u_l} = 1 + \frac{3}{2}\sqrt{3\alpha}(1-\alpha)\left[\left(\frac{\rho_l}{\rho_g}\right)^{1/3} - 1\right]. \tag{1.17}$$

Detailed analyses and comparisons of the many other models of such a type are given in the reviews of Isbin (1980) and Giot (1981). However, the model simulating both tube and nozzle flows must consider IAT, as the experiments on tube flashing flows clearly showed that the vapour is generated in jumps, but the models, which do not contain the IAT equation in partial derivatives (including Nigmatulin & Soplenkov 1980), postulate the uniformity of boiling over the flow.

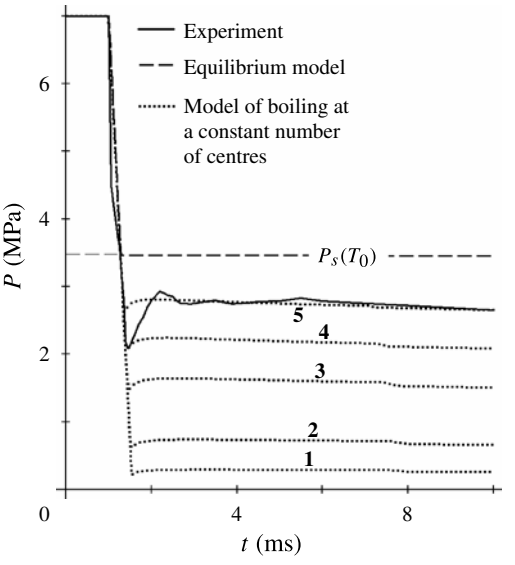

FIGURE 1. Small-scale pressure oscillograms at cross-section $x = 1.1$ m from the opened channel end. The experiment (full line) is that of Edwards & O'Brien (1970). Also shown are calculations using the equilibrium model (dashed) and the model of boiling at a constant number of centres (dotted) with (**1**) $c = 1$, (**2**) 10^2, (**3**) 10^4, (**4**) 10^5 and (**5**) 10^6 kg^{-1}.

1.2. *The 'boiling shock' phenomenon in flashing flows*

In a classic experiment on a high-pressure vessel depressurization (Edwards & O'Brien 1970), the vessel was a 4 m long horizontal tube with 7.3 cm internal diameter. The tube initially contained hot water at temperature 515 K. The pressure in the tube, $P_0 = 7$ MPa, was twice the saturation pressure and the water did not boil. The right-hand end of the tube was closed with a glass disc. On destroying the disc, liquid efflux accompanied by boiling started. A first wave of rarefaction moving with the speed of sound in a pure liquid, $\approx$1200 m s^{-1}, which transforms the liquid into a metastable state, is seen in a small-scale pressure oscillogram at the cross-section $x = 1.1$ m from the opened tube end (solid line in figure 1). The wave of rarefaction was followed by a wave of compression. These two waves formed the structure called a 'tooth of boiling' (Ivashnyov & Soplenkov 1992). Behind the tooth, a uniform pressure of 2.7 MPa, which was less than the saturation pressure (3.5 MPa) but greater than atmospheric pressure, settled all over the vessel.

In large-scale experimental pressure oscillograms, the first waves crossing the channel within 3 ms look like an instant pressure drop to $P^* = 2.7$ MPa at zero time (figure 2*a*). The pressure remained constant for a long time: only after 0.2 s did it start to decrease rapidly at the third point, and then at the fourth and fifth points. This was the second wave of rarefaction, a 'slow wave', moving with the speed of only 10 m s^{-1}.

The experimental oscillograms of the pressure and volumetric vapour fraction measured at the fourth point (solid lines in figure 3*a*,*b*) showed that the pressure drop in the 'slow wave' was accompanied by the increase in the volumetric vapour content from 0.2 to 0.9. Slow waves of boiling were observed in experiments at different initial parameters of water (Edwards & O'Brien 1970) and in experiments

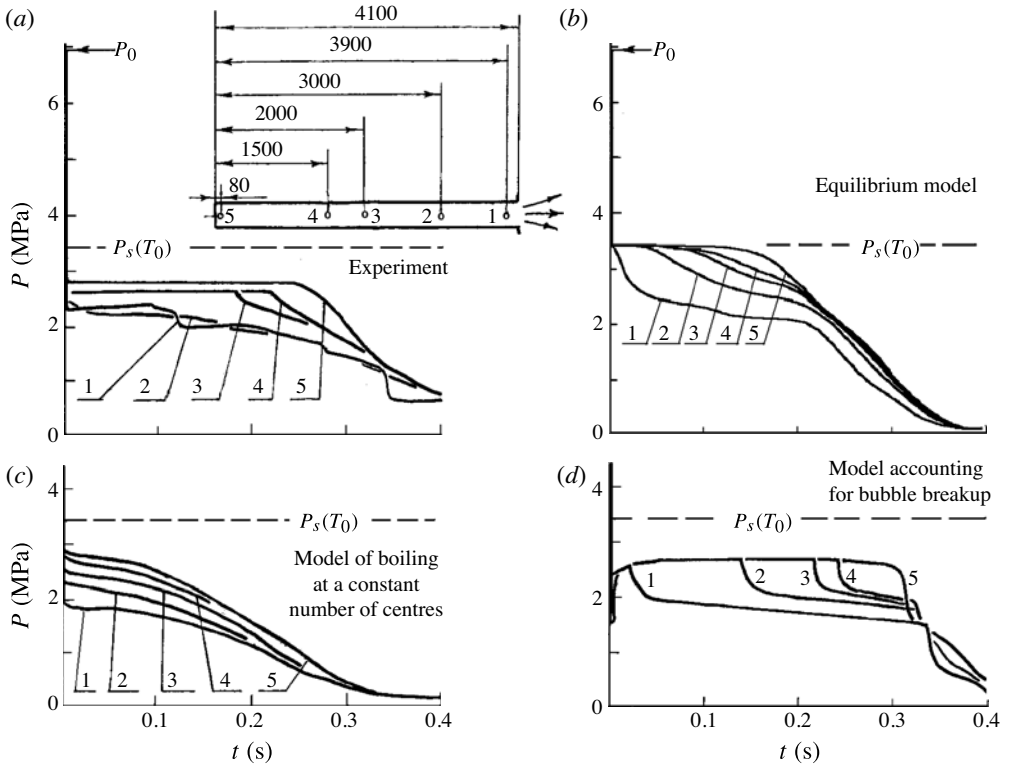

FIGURE 2. Pressure oscillograms at five different tube cross-section locations (shown in the insert to panel *a*): (*a*) the experiment of Edwards & O'Brien (1970); (*b*) calculation with the model of boiling at a constant number of centres (Nigmatulin & Soplenkov 1980); (*c*) calculation with the equilibrium model; and (*d*) calculation with the model accounting for bubble breakup (Ivashnyov *et al.* 2000).

with other fluids: CO_2 (Isaev 1980) and dichlorodifluoromethane (Winters & Merte 1979). The pressure oscillograms of Winters & Merte (1979) are presented in figure 4. The 'slow wave' analogues to that observed by Edwards & O'Brien (figure 2*a*) can be seen.

Labuntsov & Avdeev (1981) seem to have been the first to point to the phenomenon of 'boiling shocks' after high-pressure vessel decompression. Later, they showed that such shocks are also characteristic for nozzle flows (Labuntsov & Avdeev 1982). They criticized the models known at that time and proposed the 'concept' of boiling in a high-speed flow. According to the concept, liquid may stay in an overheated state within an infinitely long time until the arrival of the 'boiling shock' in which the liquid explosively boils, transforming into an equilibrium state.

In Ivashnyov *et al.* (2000), the flow with a boiling shock described above was calculated with several models. According to the equilibrium model (Ivandaev & Gubaidullin 1978), the pressure behind the first wave of rarefaction is equal to the saturation pressure, 3.5 MPa, while in the experiment it is much less, 2.7 MPa. (Compare figure 2*a*,*c* and the solid and dashed lines in figures 1 and 3.) Using the model of boiling at a constant number of centres with $c = 10^6$ kg^{-1}, one may obtain in the calculation the pressure fall to the same level as in the experiment, 2.7 MPa

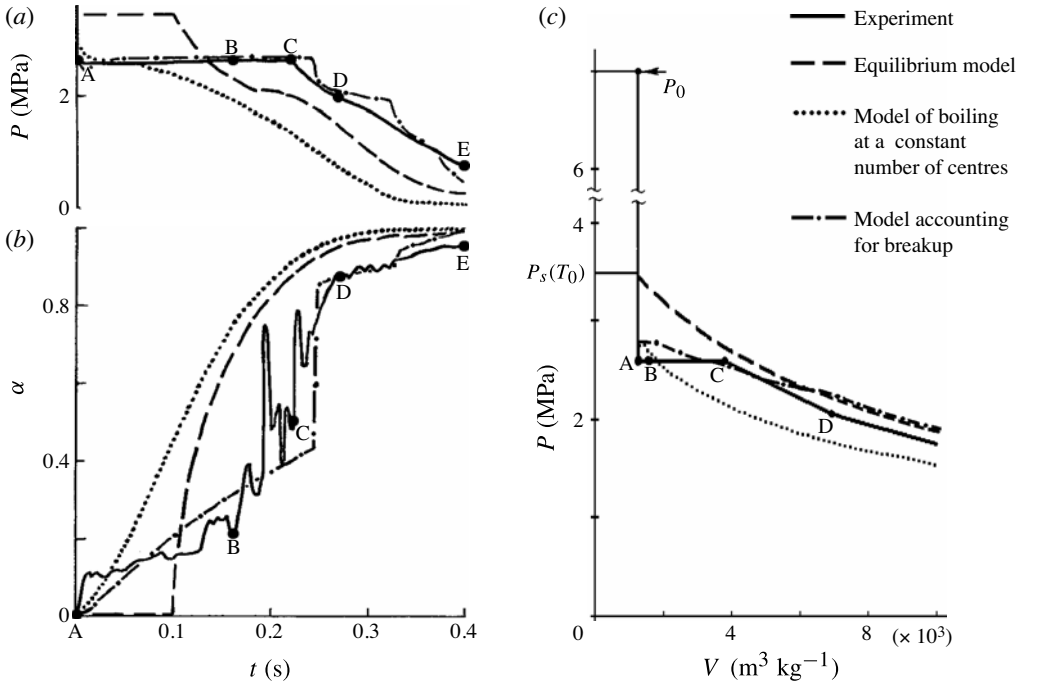

FIGURE 3. Experimental and theoretical oscillograms of (*a*) pressure and (*b*) volumetric vapour content at cross-section $x = 1.5$ m from the closed tube end (point 4 in figure 1*a*). (*c*) Expansion process in *P*–*V* (pressure–specific volume) coordinates ($V = \rho^{-1}$). Curves as in the key.

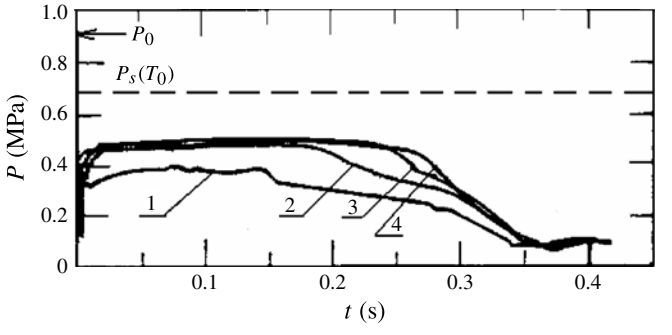

FIGURE 4. The pressure oscillograms at the cross-sections $x = 6.3$ cm, 0.428 m, 0.792 m and 1.156 m (curves 1, 2, 3 and 4, respectively) obtained in the 307th experiment on the decompression of a high-pressure vessel filled with dichlorodifluoromethane R12 (Winters & Merte 1979).

(figure 1*a*). However, the model does not predict a 'boiling shock'. According to the calculations, the subsequent pressure diminution to the atmospheric pressure occurs smoothly (see figure 2*b* and dotted lines in figure 3).

The experimental curve of the mixture expansion in *P*–*V* (pressure–specific volume) coordinates built by several points taken from figure 3(*a*,*b*) that are denoted by circles

A, B, C, D, E is presented in figure 3(*c*). From the comparison with the curve for an adiabatic expansion of an equilibrium mixture (dashed line in figure 3*c*), it is seen that the experimental curve is far from the curve of equilibrium expansion at the initial stage and approaches it within 0.3 s. On the other hand, the experimental curve of the mixture expansion is close to the curve of expansion for a non-equilibrium mixture boiling at 10^6 kg^{-1} centres (dotted line) at an initial stage and deviates significantly from it subsequently. This means that, besides a heat growth of vapour bubbles, there is an additional mechanism that intensifies the boiling and accelerates the transition of the mixture into an equilibrium state. Supposing that bubble breakup leading to the increase in the phase interface is such a mechanism, we proposed the model considering the possibility of bubble fragmentation induced by Kelvin–Helmholtz instability (Ivashnyov *et al.* 2000).

In theoretical curves of the pressure and volumetric vapour content versus time (see figure 2*d*, and dash-dotted lines in figure 3*a*,*b*) the 'jump of boiling', a thin area where the pressure falls and the volumetric vapour content increases from 0.4 up to 0.8, is clearly seen. The calculated process curve in P–V coordinates (dash-dotted lines in figure 3*c*) follows the experimental curve: it keeps to the curve of expansion for a non-equilibrium mixture boiling at a constant number of centres at the beginning and approaches the curve of equilibrium mixture expansion subsequently.

Thus, including the IAT equation in partial derivatives in the model permitted us to simulate the phenomenon of liquid evaporation in 'boiling shocks' under high-pressure tube decompression.

2. Nozzle flow simulation

For simulation, we took the experiments of Boivin (1979) in which the critical regimes of subcooled water blowdown through nozzles were studied. A system of high-pressure tanks gives hot water of constant pressure P_0 to the entrance of a Laval nozzle. On passing through the nozzle, the water boils. Two nozzles are used: a 2.3 m long 'Indira' with length-to-throat diameter ratio $l/D = 76$; and an 80 cm 'Gazeo' with $l/D = 66$. A vessel having a large volume, the silencer, creates a constant back-pressure P_{at} at the channel outlet. The pressure is measured by 12 pressure sensors installed along the nozzle. In this paper, the pressure profiles are given for three experiments. One of the experiments is carried out with 'Indira', the parameters at the nozzle entrance being: $P_0 = 6.12$ MPa, $T_0 = 545$ K and $P_{at} = 1.5$ MPa. The other two experiments are carried out with 'Gazeo', with parameters: $P_0 = 2.3$ MPa, $T_0 = 489$ K and $P_{at} = 1.7$ MPa in the first experiment; and $P_0 = 3.84$ MPa, $T_0 = 506$ K and $P_{at} = 2.7$ MPa in the second one (experiment number 9 in Boivin 1979).

The stationary flows in the nozzles are calculated by the method of 'flow set-up': the boundary conditions are fixed, the initial conditions are imposed, and the flow transition to a new regime is calculated with non-stationary equations. The distributions of the parameters for inviscid fluid at a pressure in the nozzle throat equal to the saturation pressure are imposed as initial conditions. Such initial conditions allow one to reduce significantly the time of flow in the steady-state regime, and the time of flow set-up, as the flow rate is predicted with the exactness of several dozen per cent.

2.1. *A short note on the numerical method*

Calculations with the model accounting for bubble fragmentation have required the elaboration of a special numerical scheme. The point is that numerical oscillations that

usually accompany wave simulation can provoke non-physical bubble fragmentation and distort the solution significantly. The usual method to suppress these oscillations, the introduction of a pseudo-viscosity, cannot be used, as it stretches the wave front and suppresses bubble breaking. A method to exclude the numerical pulsations in the wave calculation that still permits the wave structure to be calculated precisely has been worked out. The description of the method is given in appendix B of Ivashnyov *et al.* (2000).

For a nozzle flow calculation, the conservation of the mass flux ρuF and flow strength $i + u^2/2$ along the nozzle in the steady-state regime of efflux should be provided. To keep the relative non-uniformity at the level of 0.01 %, the dimension of a numerical cell was taken to be 0.2 mm.

2.2. *The equilibrium model*

The temperatures, pressures and velocities of the liquid and vapour phases are considered equal. A steady-state flow of an equilibrium mixture through a nozzle is described by the following equations:

$$G = \rho uF = \text{const.}, \tag{2.1}$$

$$\frac{\mathrm{d}P}{\mathrm{d}x} = \frac{\rho u^2 F_x/F - \xi(1 + \rho u^2\varphi/T)\rho|u|u/(2D)}{1 - u^2/a_e^2}, \quad F_x = \frac{\mathrm{d}F}{\mathrm{d}x}, \tag{2.2}$$

$$\frac{\mathrm{d}S}{\mathrm{d}x} = \xi\frac{|u|}{2DT}u. \tag{2.3}$$

The coefficient of wall friction ξ is approximated by the dependence on Reynolds number obtained for a pure liquid flow in a straight channel, given by

$$\xi = \begin{cases} 64Re_D^{-1}, & Re_D \leqslant 2300, \\ 0.0278, & Re_D > 2300, \end{cases} \quad Re_D = \frac{D\rho_l u}{\mu_l}, \tag{2.4}$$

where Re_D is the Reynolds number for the flow, and μ_l is the coefficient of dynamic viscosity of the liquid.

The equation of state for an equilibrium mixture is a piecewise continuous dependence between the mixture density, pressure and entropy. It consists of two parts. At the point of their intersection (the point of boiling inception), the derivative of density with respect to pressure can be broken down as

$$\rho = \begin{cases} \rho_l(P, S_l), & P \geqslant P_s(S_l), \\ \left(\dfrac{1}{\rho_l} + \varphi(P)(S - S_l)\right)^{-1}, & P < P_s(S_l), \end{cases} \quad \varphi(P) = \left(\frac{\partial T}{\partial P}\right)_{sat}, \tag{2.5}$$

where $\varphi(P)$ is the derivative of temperature with respect to pressure on the line of saturation; P_s is the saturation pressure; and S and S_l are the mixture and liquid entropies.

The first part of (2.5) is the equation of state for a pure liquid, and the second part is that for an equilibrium mixture. The latter follows from the equality of thermodynamic potentials of liquid and vapour on the line of saturation (Vaisman 1967; Sivuchin 1979). The isentropic curve for an equilibrium mixture is shown by the dashed line in figure 3(*c*).

The equations for the speed of sound in the liquid and two-phase mixture are obtained by differentiating (2.5) with respect to pressure at of constant entropy,

$S = \text{const.}$, thus

$$a_e = \left(\frac{\partial \rho}{\partial P}\right)_S^{-1/2} = \begin{cases} a_l, & \text{at } P \geqslant P_s, \\ \left\{\left(\dfrac{\rho}{\beta}\right)^2 - \rho\left[\left(1 - \dfrac{\rho}{\rho_l}\right)\dfrac{1}{\varphi}\left(\dfrac{\partial^2 T}{\partial P^2}\right)_{sat} - \dfrac{\rho\varphi}{\rho_l T}\left(\rho_l\left(\dfrac{\partial i_l}{\partial P}\right)_{sat} - 1\right)\right]\right\}^{-1/2}, & \text{at } P < P_s. \end{cases} \tag{2.6}$$

The speed of sound in the liquid is $a_l \sim 1000$ m s^{-1}; the speed of sound in a two-phase mixture is less by an order of magnitude, a_e–$10 \div 100$ m s^{-1}. At the point of flashing inception, the speed of sound changes stepwise from the speed of sound in a pure liquid down to the speed of sound in an equilibrium two-phase mixture.

Neglecting the dependence of the liquid density on temperature, and considering the isotherms built in P–V coordinates to be straight lines near the saturation curve, one can rewrite the equation of state for the liquid as

$$\frac{1}{\rho_l} = k - \frac{P}{\beta^2}, \tag{2.7}$$

$$\beta = \beta(T_0) = \text{const.}, \quad k = \frac{1}{\rho_{ls}(T_0)} + \frac{P_s(T_0)}{[\beta(T_0)]^2} = \text{const.}, \tag{2.8}$$

where $P_s(T_0)$, $\rho_{ls}(T_0)$ and $\beta(T_0)$ are the pressure, liquid density and the coefficient of isothermal compressibility of the liquid on the line of saturation at the initial liquid temperature T_0.

The caloric equation for the liquid follows from its equation of state (2.7):

$$i_l(P, T_l) = i_{ls}(T_l) + k(P - P_s(T_l)) - \frac{P^2 - P_s^2(T_l)}{2\beta^2}, \tag{2.9}$$

where i_l is the liquid enthalpy; $i_{ls} = c_s(T_l - b_s)$ is the liquid enthalpy on the line of saturation; and $c_s = 5000$ m^2 s^{-2} K^{-1} and $b_s = 305$ K are approximate parameters.

The isobaric specific heat of the liquid is determined by differentiating (2.9):

$$c_l = \left(\frac{\partial i_l}{\partial T}\right)_P = c_s - \frac{1}{\varphi(P_s(T))}\left(k - \frac{P_s(T)}{\beta^2}\right). \tag{2.10}$$

The liquid entropy is a function of its temperature and is calculated as

$$S_l(T_l) = S_{l0} + \int_{T_0}^{T_l} c_l \frac{\mathrm{d}T_l}{T_l}, \tag{2.11}$$

where S_{l0} is the liquid entropy at temperature T_0.

Within a wide range of temperatures, 450 K $\leqslant T_s \leqslant$ 590 K, the simple relationships

$$\rho_g = \frac{P}{a_g^2}, \quad i_g = 2.8 \times 10^6 \text{ m}^2 \text{ s}^{-2} \tag{2.12}$$

describe the vapour density and enthalpy on the line of saturation with a maximal relative error of 2 %. Here $a_g^2 = 2 \times 10^5$ m^2 s^{-2} is the approximation constant. Thus, the equilibrium model has no free parameters.

A singular point corresponding to the vanishing condition for the denominator of (2.2) ($u = a_e$) at a location where the numerator vanishes can appear in a calculation. The flow regime with a singular point is a critical one. The critical mass flow rate is the maximal possible flow rate for the given channel geometry and for the given P_0 and T_0. Since the numerator can become equal to zero solely at $F_x > 0$, the singular point is placed in the nozzle diffuser.

The calculation of the 'flow set-up' in the 'Indira' nozzle with the equilibrium model is presented in the left part of figure 5. The approximate (smoothed) nozzle profile is shown in figure 5(*a*). The calculated mass flux, $G_t = 15.4$ kg s^{-1}, corresponds to the experimental value, $G_{ex} = 18.8$ kg s^{-1}, with the relative error

$$\varepsilon = \frac{G_t - G_{ex}}{G_{ex}} \times 100\,\% \approx -18\,\% \tag{2.13}$$

(circles and dashed lines in figure 5*c*, left).

According to the calculations, the pressure decreases to the saturation pressure in the nozzle throat (figure 5*b*, left). The mixture velocity increases up to the equilibrium speed of sound, $M_e = u/a_e = 1$, at the beginning of the diffuser (figure 5*d*, left). Downstream of the critical cross-section, the flux continues to accelerate up to the jump of compression in which the flow slows down and transforms into a subsonic one.

The flow set-up in 'Gazeo' at the conditions of the first experiment calculated with the equilibrium model is presented in the left part of figure 6. The relative error of the model predictions evaluated from calculated and experimental mass flux values, $G_t = 1.34$ and $G_{ex} = 1.9$ kg s^{-1}, is higher: $\varepsilon \approx -30\,\%$. The flow scheme is the same: in the throat, the pressure diminishes to the saturation pressure (figure 6*b*, left), and the flow overcomes a sound barrier $M_e = 1$ at the beginning of the diffuser (figure 6*d*, left). The back-transition of the flow into a subsonic one occurs in the jump of compression, which is located downstream in the diffuser.

The 'flow set-up' in 'Gazeo' at the conditions of the second experiment (no. 9 in Boivin 1979) calculated with the equilibrium model is presented in the left part of figure 7 (left). The calculated and experimental mass fluxes are $G_t = 3.05$ and $G_{ex} = 3.93$ kg s^{-1}. The relative error of the model predictions is $\varepsilon \approx -22\,\%$.

2.3. *The model of boiling at a constant number of bubbles*

The liquid is assumed to boil only on nucleation centres that exist within it and the number of bubbles per unit mixture mass, $c = n/\rho$, remains constant. The model considers the pressures and velocities in the liquid and vapour phases to be equal, but temperatures are considered to be different. The parameters in a bubble are assumed to be uniform and equal to the parameters on the line of saturation. For pressures smaller than the critical pressure, the vapour density is assumed to be much less than the liquid density. The model consists of (1.1)–(1.6), the stationary analogue of which is

$$G = \rho u F = \text{const.}, \tag{2.14}$$

$$\frac{\mathrm{d}P}{\mathrm{d}x} = \frac{\rho u[uF_x/F - \xi|u|/(2D) - J(1/\rho_g - 1/\rho_l)]}{1 - u^2/a_f^2}, \tag{2.15}$$

$$\frac{\mathrm{d}\chi}{\mathrm{d}x} = \frac{jc}{u}, \quad \chi = \frac{\rho_g \alpha}{\rho}, \tag{2.16}$$

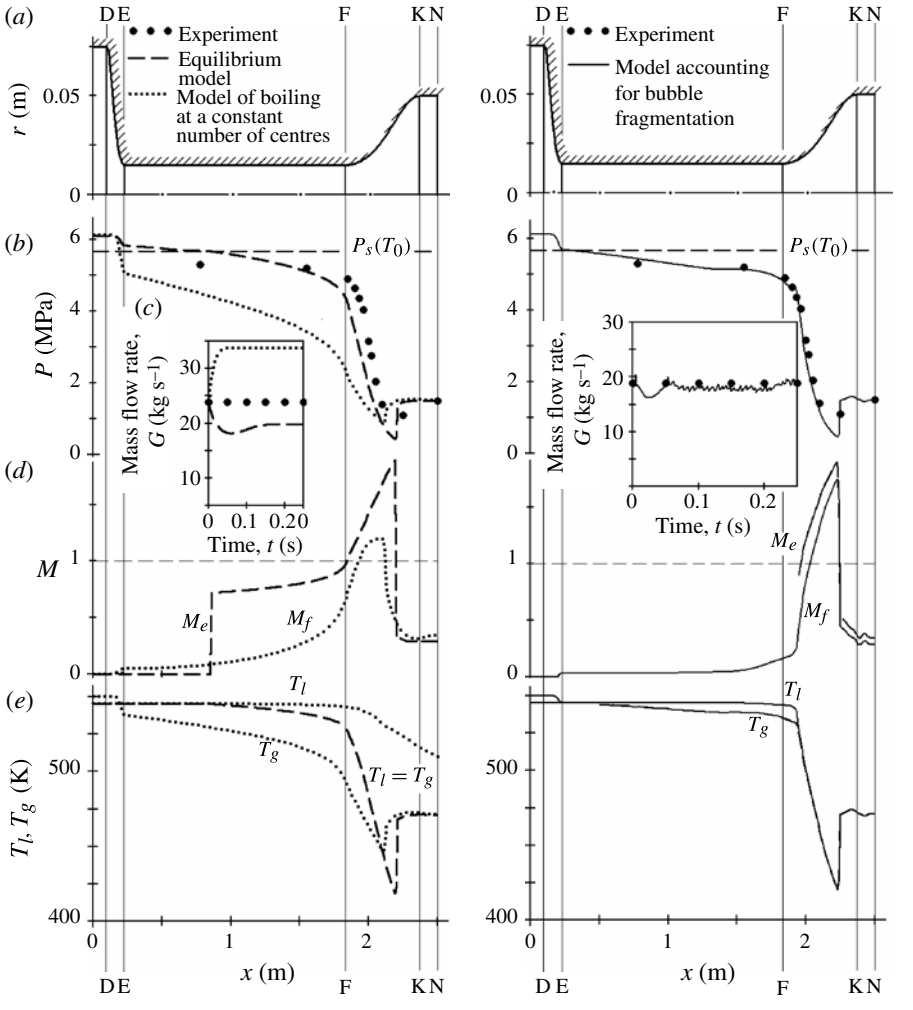

FIGURE 5. Calculation of the flow set-up in the 'Indira' nozzle, compared with experimental data. The left part shows the calculations using the equilibrium model and the model of boiling at a constant number of centres $c_0 = 10^6\ \mathrm{kg}^{-1}$. The right part shows the calculation using the model accounting for bubble breakup with parameters $c_0 = 4 \times 10^5\ \mathrm{kg}^{-1}$ and $We^* = 1$. (*a*) The nozzle profile; (*b*,*d*,*e*) the profiles of (*b*) pressure, (*d*) Mach numbers $M_e = u/a_e$ and $M_f = u/a_f$ and (*e*) temperature at $t = 0.4$ s; and (*c*) time dependence of mass flux through the cross-section E–E.

$$I = i + \frac{u^2}{2} = \text{const.}, \tag{2.17}$$

$$c = \frac{n}{\rho} = \text{const.}, \tag{2.18}$$

$$F_x = \frac{\mathrm{d}F}{\mathrm{d}x}, \quad a_f = \left[\rho\left(\frac{(1-\alpha)\rho_l}{\beta^2} + \frac{\alpha}{P}\right)\right]^{-1/2}, \quad J = jn, \tag{2.19}$$

where a_f is a 'frozen' speed of sound, which characterizes the mixture compressibility in the absence of mass exchange between phases; and j is the intensity of liquid

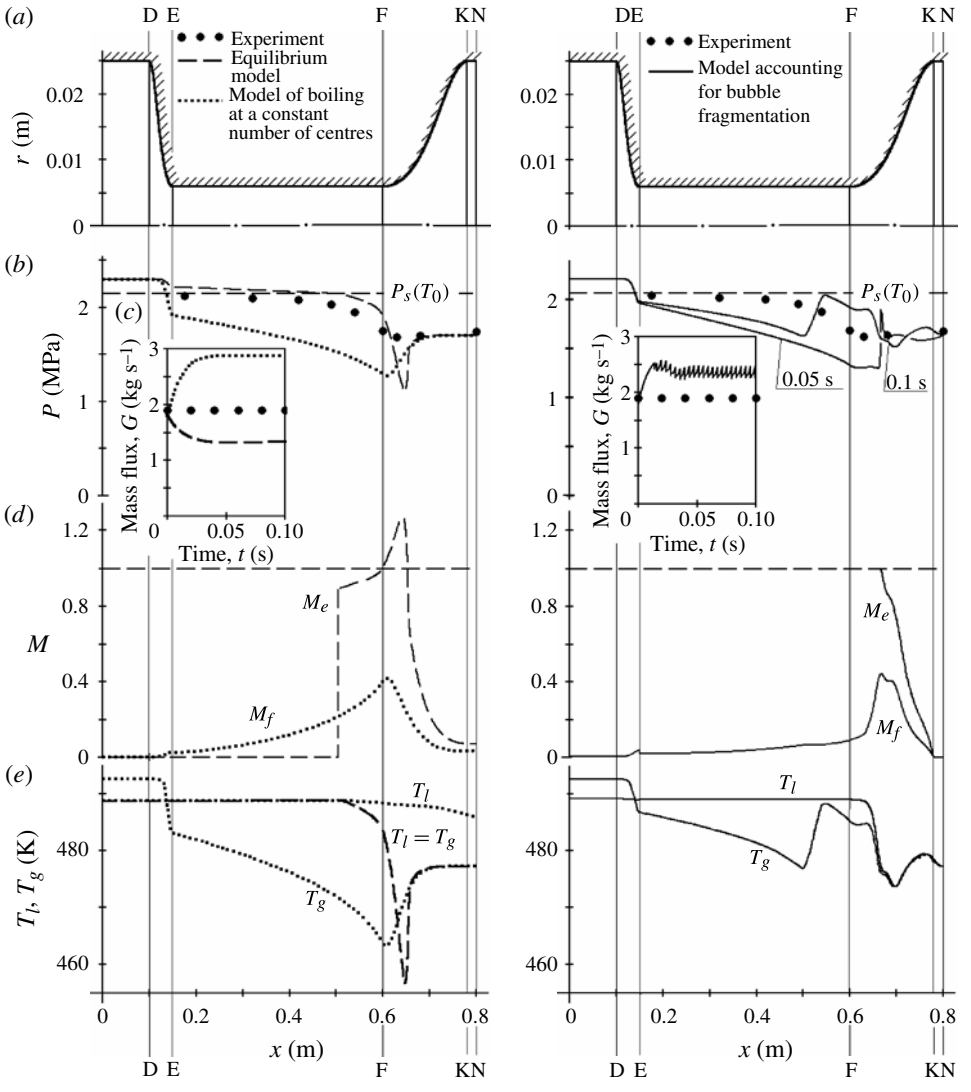

FIGURE 6. Calculation of the flow set-up in the 'Gazeo' nozzle for the conditions of the first experiment, compared with experimental data. The left part shows the calculations using the equilibrium model and the model of boiling at a constant number of centres $c_0 = 10^6$ kg^{-1}. The right part shows the calculation using the model accounting for bubble breakup with parameters $c_0 = 4 \times 10^5$ kg^{-1} and $We^* = 1$. (*a*) The nozzle profile; (*b*,*d*,*e*) the profiles of (*b*) pressure, (*d*) Mach numbers $M_e = u/a_e$ and $M_f = u/a_f$ and (*e*) temperature at $t = 0.1$ s; and (*c*) time dependence of mass flux through the cross-section E–E.

evaporation into a bubble, which is determined as

$$j = 2\pi D_l a \rho_l \, Ja \, Nu, \quad D_l = \lambda_l \, (\rho_l c_l)^{-1}, \tag{2.20}$$

where D_l is the coefficient of thermal diffusivity of the liquid.

Scriven (1959) has shown that a self-similar temperature profile is settled over a bubble growing in an overheated liquid within the time $\sim (a\,Nu)^2 \, D_l^{-1}$. The self-similar

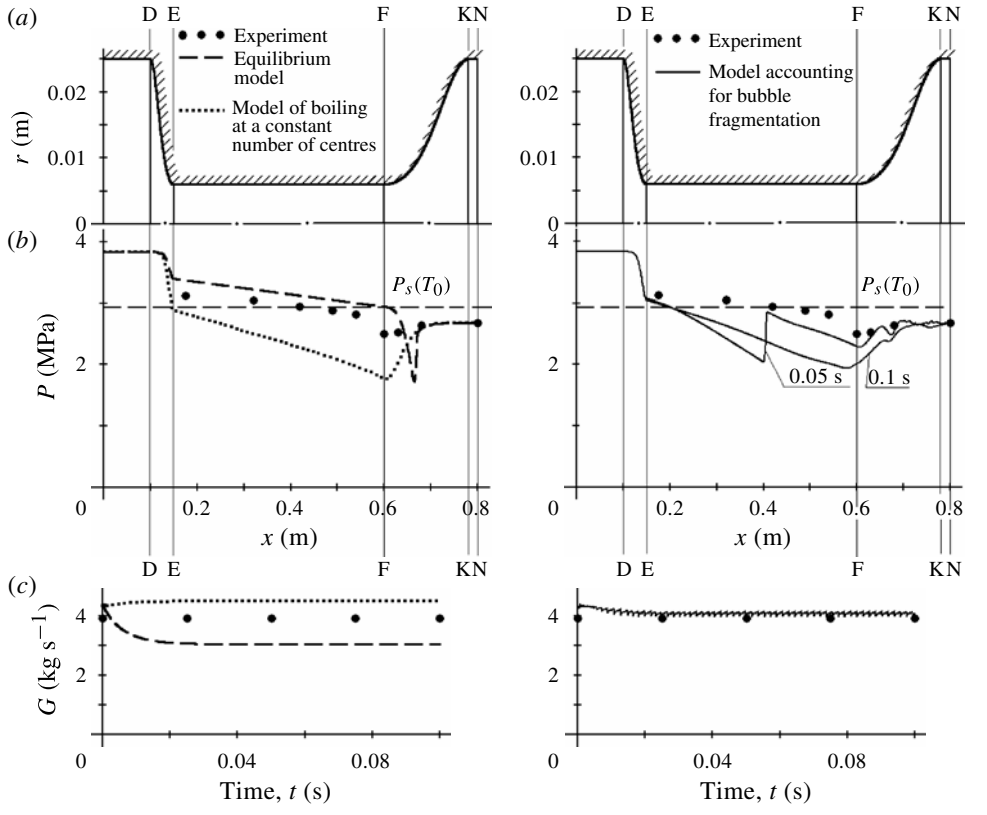

FIGURE 7. Calculation of the flow set-up in the 'Gazeo' nozzle for the conditions of the second experiment, compared with experimental data. The left part shows the calculations using the equilibrium model and the model of boiling at a constant number of centres $c_0 = 10^6$ kg^{-1}. The right part shows the calculation using the model accounting for bubble breakup with parameters $c_0 = 4 \times 10^5$ kg^{-1} and $We^* = 1$. (*a*) The nozzle profile; (*b*) the pressure profiles; and (*c*) time dependence of mass flux through the cross-section E–E.

solution permits one to define the link between the dimensionless temperature gradient in the liquid adjoining the bubble surface, a Nusselt number Nu, and the dimensionless liquid overheat, a Jacob number, Ja:

$$Nu = 2 + \left(\frac{6Ja}{\pi}\right)^{2/3} + \frac{12Ja}{\pi}, \quad Ja = \frac{c_l \rho_l \left(T_l - T_g\right)}{\rho_g h}. \tag{2.21}$$

From equation (2.15), it follows that the critical point where the flow and sonic velocities are equal ($u = a_f$) can be placed in the nozzle diffuser only.

The only free model parameter, the number of boiling centres per mixture mass unit $c = 10^6$ kg^{-1}, is taken from the adjustment of the model with the experiment on a tube decompression (figure 1*a*).

The calculations of the flow through the 'Indira' nozzle using the non-equilibrium model are presented in the left part of figure 5 by dotted lines. A calculated mass flow rate through the nozzle is 1.5 times greater than the experimental one, $G_t \approx 29$ kg s^{-1} (figure 5*c*, left). The theoretical pressure profile also differs significantly from the experimental one (figure 5*b*, left). Thus, without modifying the model free parameter,

the accuracy of the predictions of the model of boiling at a constant number of centres is 2.5 times lower than the accuracy of simpler equilibrium model.

According to the calculation, the pressure decreases to the saturation pressure ($P_s(T_0)$) in the convergent section. In the diffuser, the flow velocity increases up to a 'frozen' speed of sound: $M_f = u/a_f = 1$ (figure 5*d*, left). Behind the critical cross-section, the flow continues to accelerate up to the jump of compression in which the flow slows down and transforms into a subsonic one (figure 5*b*,*d*, left). The distributions of phase temperatures along the channel show that the mixture remains essentially non-equilibrium all over the channel length (figure 5*e*, left).

The calculation of the efflux through the shorter nozzle 'Gazeo' under the conditions of the first experiment is shown by dotted lines in the left part of figure 6. The theoretical pressure profile differs essentially from the experimental one. The relative error of the mass flux prediction is the same as for 'Indira' calculations with this model, $\varepsilon \approx +50\,\%$. The Mach number profile (figure 6*d*, left) suggests that the flow velocity does not exceed the speed of sound in the nozzle whereas, according to the experiment, the flow is critical. Calculated temperature profiles show that the mixture leaves the nozzle being essentially non-equilibrium (figure 6*e*, left).

The calculation of the flow in 'Gazeo' under the conditions of the second experiment is shown by dotted lines in the left part of figure 7. The relative error of the mass flow rate prediction is $+14\,\%$.

Thus, for both nozzles, 'Indira' and 'Gazeo', the experimental values of the mass flow rate and the pressure profiles are between the predictions of an equilibrium model and the model of boiling at a constant number of centres (figures 5*c*–7*c*). This means that the bubble number is between 10^6 kg^{-1} and infinity. The number of boiling centres chosen to predict tube decompression, 10^6 kg^{-1}, is thus not suitable for simulation of the flow in the 'Indira' nozzle in spite of the same fluid and close initial parameters. This suggests that the bubble number is not constant in flashing flows.

2.4. *The model accounting for bubble breakup*

Boiling is considered to start up at centres of nucleation. The pressures in the phases are considered to be equal; the parameters in a bubble are uniform and equal to the parameters on the line of saturation; the vapour density is much less that the liquid density; the phase slip $|u_g - u_l| \ll u_l$.

The model includes equations of conservation for mixture mass, momentum and energy (1.1)–(1.3), the equation of vapour mass balance (1.5), the IAT equation (1.9) and the equation for bubble momentum balance (1.10).

The intensity of bubble breakup ψ is defined with a relaxation ratio:

$$\psi = \frac{c^* - c}{\tau^*}, \tag{2.22}$$

where c^* is the number of bubbles that would be formed if the fragmentation were instantaneous, and τ^* is the characteristic fragmentation time.

The parameters c^* and τ^* are specified using the solution of the problem about the rise in amplitude of a small harmonic perturbation with wavelength λ arising on a plane interphase boundary (Lamb 1957; Birkhoff 1960; Ishii & Hibiki 2006):

$$\xi = K \exp\left[ht - \mathrm{i}\frac{2\pi}{\lambda}x\right], \quad h(\lambda) = \pm\sqrt{\frac{4\pi^2}{\lambda^2}\frac{\rho_g(u_g - u_l)}{\rho_l} - \frac{8\pi^3}{\lambda^3}\frac{\sigma}{\rho_l}}. \tag{2.23}$$

From the condition that a bubble is divided by the wave with the fastest growing amplitude,

$$\lambda^{**} = \frac{3\pi\sigma}{\rho_g (u_g - u_l)^2}, \tag{2.24}$$

and the condition that the length of the wave cannot exceed the bubble diameter, $\lambda^{**} \leqslant 2a$, one obtains the criterion of surface stability of a bubble overflowing by fluid, the Weber number,

$$We = \frac{2a\rho_g (u_g - u_l)^2}{\sigma}, \tag{2.25}$$

and the evaluation of its critical value, $We^* = 3\pi$.

The number of fragments appearing as a result of bubble breakup (c^*/c) is determined as the ratio of the bubble diameter to the length of the wave causing breakup, and a characteristic time of breakup is adopted to be the time of 'e' time rise (e = 2.7...) in amplitude of the perturbation with wavelength λ^{**}:

$$\frac{c^*}{c} = \frac{2a}{\lambda^{**}} = \frac{We}{We^*}, \quad \tau^* \sim \frac{1}{h(\lambda^{**})} = \sqrt{\frac{\rho_l a^3}{\sigma}\left(\frac{We}{We^*}\right)^3}. \tag{2.26}$$

The difference in phase velocities in the equation for We is determined from the equation of motion of an individual dispersed unit (1.10). However, formula (1.10) obtained for a single bubble predicts the acceleration of breaking bubbles with diminishing radii. This contradicts the physical reality, as the total volume of bubbles and, consequently, the total virtual mass does not vary under the breaking process. Thus bubble breakup should not lead to bubble acceleration.

To exclude the non-physical effect, we will pass on from the parameters characterizing a single bubble to the mean parameters for the vapour phase. From the mass balance equation for a single (not fragmenting) bubble

$$\frac{\mathrm{d}_g}{\mathrm{d}t}\left(\rho_g \frac{4}{3}\pi a^3\right) = j, \tag{2.27}$$

we obtain

$$\frac{\mathrm{d}_g}{\mathrm{d}t}\left(\frac{4}{3}\pi a^3\right) = \frac{j}{\rho_g} - \frac{4\pi a^3}{3\rho_g}\frac{\mathrm{d}_g \rho_g}{\mathrm{d}t}. \tag{2.28}$$

Multiplying (2.28) by $\rho_l(u_g - u)/2$ and summing up the result with (1.10), we will obtain the equation for the difference in phase velocities:

$$\frac{\mathrm{d}_g}{\mathrm{d}t}\left(\frac{u_g - u}{\rho_g}\right) = \frac{2}{\rho_g}\frac{\mathrm{D}u}{\mathrm{D}t} - \frac{3}{4a}\left[c_\mu |u_g - u| + \frac{j}{\pi a^2 \rho_g}\right]\frac{u_g - u}{\rho_g}. \tag{2.29}$$

Taking into account the assumption about the smallness of the phase slip $|u_g - u_l| \ll u_l$, we replace the material derivative following the bubbles $\mathrm{d}_g/\mathrm{d}t$ by the material derivative following the mixture $\mathrm{D}/\mathrm{D}t$. Assuming $\mathrm{d}_g/\mathrm{d}t = \mathrm{D}/\mathrm{D}t$, one obtains:

$$\frac{\mathrm{D}}{\mathrm{D}t}\left(\frac{u_g - u}{\rho_g}\right) = \frac{2}{\rho_g}\frac{\mathrm{D}u}{\mathrm{D}t} - \frac{3}{4a}\left[c_\mu |u_g - u| + \frac{j}{\pi a^2 \rho_g}\right]\frac{u_g - u}{\rho_g}. \tag{2.30}$$

Equation (2.30), which excludes the above-mentioned deficiency since the radius of a discrete bubble does not enter into it, is a generalized equation of the balance of

forces acting on a bubble. From (2.30), it follows that the liquid acceleration is the only reason for the disturbance of the equality in the phase velocities. The second term on the right-hand side of (2.30) is 'responsible' for the velocity equilibrium renewal.

The coefficient of viscous resistance c_μ is defined as follows:

$$c_\mu = \begin{cases} \dfrac{16}{Re}, & Re \leqslant 10.9, \\ \dfrac{48}{Re}\left(1 - \dfrac{2.2}{\sqrt{Re}}\right), & 10.9 < Re \leqslant 1000, \\ 4.466 \times 10^{-2}, & Re > 1000, \end{cases} \qquad Re = 2a\rho_l \frac{|u_g - u|}{\mu_l}, \tag{2.31}$$

where Re is the bubble Reynolds number.

Thus the boiling flow model accounting for bubble breakup initiated by Kelvin–Helmholtz instability includes: the balance equations for the mixture mass, momentum and energy (1.1)–(1.3), and vapour mass (1.5); the IAT equation (1.9) with bubble breakup scheme (2.22)–(2.26); the equation for the phase slip (2.30); the equations of state for the liquid and vapour phases (2.7)–(2.14); the expression for the coefficient of the flow friction on walls ξ (2.4); and the ratios (2.20) and (2.21) determining the intensity of the liquid evaporation into a bubble, j.

A stationary analogue of the model accounting for bubble breakup is as follows:

$$G = \rho u F = \text{const.}, \tag{2.32}$$

$$\frac{\mathrm{d}P}{\mathrm{d}x} = \frac{\rho u\{uF_x/F - \xi|u|/(2D) - jn(\rho_g^{-1} - \rho_l^{-1})\}}{1 - u^2/a_f^2}, \quad F_x = \frac{\mathrm{d}F}{\mathrm{d}x}, \tag{2.33}$$

$$\frac{\mathrm{d}\chi}{\mathrm{d}x} = \frac{jc}{u}, \quad \chi = \frac{\rho_g \alpha}{\rho}, \tag{2.34}$$

$$I = i + \frac{u^2}{2} = \text{const.}, \tag{2.35}$$

$$\frac{\mathrm{d}}{\mathrm{d}x}\left(\frac{\Delta u}{\rho_g}\right) = -\frac{2}{\rho_g \rho u}\frac{\mathrm{d}P}{\mathrm{d}x} - \frac{3}{4a}\left[c_\mu|\Delta u| + \frac{j}{\pi a^2 \rho_g}\right]\frac{\Delta u}{\rho_g u}, \tag{2.36}$$

$$\frac{\mathrm{d}c}{\mathrm{d}x} = \frac{\psi}{u}, \tag{2.37}$$

where $\Delta u = u_g - u$ is the phase slip.

The model has two free parameters, the number of initial bubbles and the critical Weber number, which are adopted to be the same as those used to simulate a tube decompression: $c_0 = 4 \times 10^5$ kg^{-1} and $We^* = 1$.

The calculation of the 'flow set-up' in the 'Indira' nozzle is shown in the right-hand part of figure 5. It is seen that the flow goes over on a vibration regime. The vibration frequency is $\approx$200 s^{-1}. Thus, a good correspondence is achieved with the experiment of a calculated pressure profile and a mean mass flow rate (figure 5*b*,*c*, right). The relative error of the mass flux prediction is $\varepsilon \approx -2\,\%$. This model predicts the formation of the 'jump of boiling' at the beginning of the diffuser ($x \approx 1.9$ m). In the jump, the mixture converts into an equilibrium state (the liquid and vapour temperatures equalize, figure 5*e*), and the flow velocity becomes equal to the equilibrium sound velocity ($M_e = u/a_e \approx 1$). Behind the jump of boiling, the flow continues to accelerate up to the jump of compression where the flow velocity decreases and the flux becomes subsonic again.

Fluxes	Relative error (%), $(V_t - V_{ex})V_{ex}^{-1} \times 100\,\%$		
	Equilibrium model	Model of boiling at constant number of bubbles	Model accounting for bubble breakup
Tube decompression, $P_0 = 7$ MPa, $T_0 = 515$ K	+30	0	0
Nozzle 'Indira', $P_0 = 6.12$ MPa, $T_0 = 545$ K, $l/D = 76$	−18	+50	−2
Nozzle 'Gazeo', $P_0 = 2.3$ MPa, $T_0 = 489$ K, $l/D = 66$ (first experiment)	−30	+50	+20
Nozzle 'Gazeo', $P_0 = 3.84$ MPa, $T_0 = 506$ K, $l/D = 66$ (second experiment)	−22	+14	+4

TABLE 1. Accuracy of flashing flow simulations.

The 'flow set-up' in the 'Gazeo' nozzle under the conditions of the first experiment is shown in the right-hand part of figure 6. This flow goes out on a self-oscillated regime as well. The amplitude of the vibrations is essentially higher than in 'Indira'. The correspondence with the experiment in the pressure profile and mean mass flux is worse: the relative error of the mass flux prediction is $\varepsilon \approx +20\,\%$. The jump of boiling is formed in the diffuser as in the case of the 'Indira' flow. In the jump, phase temperatures equalize (figure 6*e*, right) and the flow velocity runs up to the equilibrium speed of sound ($M_e \approx 1$, see figure 6*d*, right): the efflux regime is a critical one. Behind the jump, the Mach number M_e decreases.

The simulation of the second experiment with 'Gazeo' is given in the right-hand part of figure 7. The relative error of the mass flux prediction is $\varepsilon \approx +4\,\%$.

Thus, for temperature T_0 at the nozzle inlet greater than the initial liquid temperature in the experiment used for the model fitting (Edwards & O'Brien 1970), the model proposed underpredicts the mass flow rate and overpredicts it for the nozzle flow with T_0 less than the initial liquid temperature.

In table 1 are shown the relative errors of the predictions for a tube and for the nozzle flows calculated by the three models: an equilibrium model, a non-equilibrium model with boiling at a constant number of centres, and a model accounting for bubble fragmentation (Ivandaev & Gubaidullin 1978; Nigmatulin & Soplenkov 1980; Ivashnyov *et al.* 2000). For the tube decompression, the error is determined from the accuracy of the prediction of the pressure level established at an initial stage of the decompression. For nozzle flows, the error is determined from the mass flow rate prediction.

It is seen that the model accounting for bubble breakup ensures the closest correspondence to experimental data.

3. Detailed investigation of oscillatory flow

In figure 8, a detailed investigation of an oscillatory efflux through 'Indira' with the model accounting for bubble breakup is presented. It is seen that, near the diffuser entrance, the Weber number rises to its critical level $We = We^*$. Bubble breakup

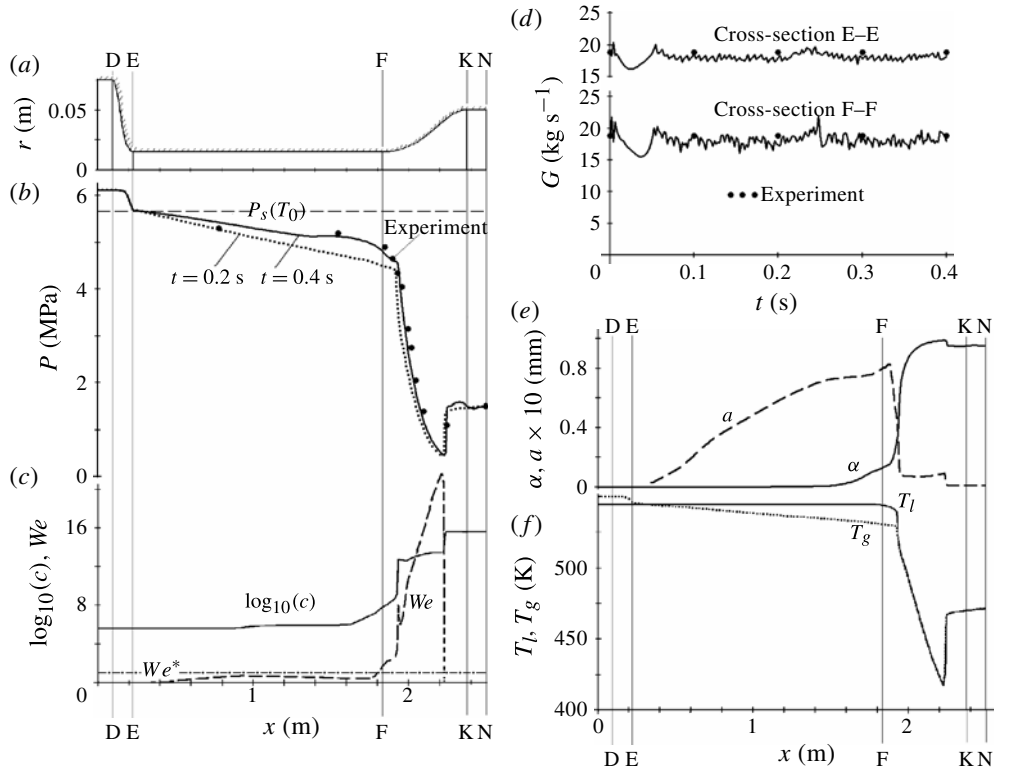

FIGURE 8. Calculation of the oscillatory flow through 'Indira' with the model accounting for bubble breakup. (*a*) Nozzle profile. (*b*) Experimental and calculated pressure profiles at $t = 0.2$ and 0.4 s. (*c*) Distributions for the Weber and bubble numbers at $t = 0.4$ s. (*d*) Experimental and calculated mass flow rate. (*e*,*f*) Profiles of (*e*) volumetric vapour fraction and bubble radius and (*f*) phase temperatures at $t = 0.4$ s.

begins, and the number of centres increases from the initial value, $c_0 = 4 \times 10^5$, up to 10^{13} kg^{-1} (figure 8*c*). A sharp increase in the bubble number leads to an explosion-like evaporation: the volumetric vapour fraction rises from 0 up to 0.9 (figure 8*e*). The phase temperatures equalize (figure 8*f*). All the changes take place within a distance of $\sim$1 cm. An analogous wave structure that is realized under a high-pressure vessel decompression (figures 2 and 3) was called a 'slow wave of boiling'.

4. Mechanism of autovibrations

The flow going out into a self-oscillation regime means that a stationary regime of efflux is either lacking or is not stable. Let us now calculate a steady-state nozzle flow with bubble fragmentation. For its analysis, we will need to calculate a steady-state flow with no breakup and the structure of a boiling wave.

4.1. *Structure of the boiling wave*

To analyse the boiling wave structure, we will go over to a moving coordinate system (t, z) fitted to the wave, with $z = x + Dt$, where D is the velocity of the wave displacement. Estimations show that, in this coordinate system, the partial time

derivatives are negligibly small:

$$\frac{\partial}{\partial t} \sim \frac{1}{T} \sim 10^2 \text{ s}^{-1} \ll (u + D)\frac{\partial}{\partial z} \sim \frac{(u^* + D)}{l} \sim 10^4 \text{ s}^{-1}. \tag{4.1}$$

Here $T \sim 10^{-2}$ s is the oscillation period, $u^* \sim 100$ m s^{-1} is the characteristic flow velocity, and $l \sim 10^{-2}$ m is the width of the wave.

Neglecting the change in the channel cross-sectional area within the wave front and the flow friction on the channel walls in a stationary analogue of the model accounting for bubble fragmentation (2.32)–(2.37) and replacing coordinate x by z, we obtain the system of model equations in the moving frame (t, z):

$$g = \rho v = \text{const.}, \tag{4.2}$$

$$R = gv + P = \text{const.}, \tag{4.3}$$

$$I = i + \frac{v^2}{2} = \text{const.}, \tag{4.4}$$

$$\frac{\mathrm{d}P}{\mathrm{d}z} = -g\frac{jn(1/\rho_g - 1/\rho_l)}{1 - u^2/a_f^2}, \tag{4.5}$$

$$\frac{\mathrm{d}}{\mathrm{d}z}\left(\frac{\Delta v}{\rho_g}\right) = -\frac{2}{\rho_g g}\frac{\mathrm{d}P}{\mathrm{d}z} - \frac{3}{4a}\left[c_\mu|\Delta v| + \frac{j}{\pi a^2 \rho_g}\right]\frac{\Delta v}{\rho_g v}, \tag{4.6}$$

$$\frac{\mathrm{d}c}{\mathrm{d}z} = \frac{\psi}{v}, \tag{4.7}$$

where $v = u + D$ is the flow velocity in the moving frame; and $\Delta v = u_g - u$ is the difference in phase velocities.

At point $z = 0$, all the parameters except the oncoming flow velocity v^* are taken from the numerical calculations given in figure 8: $P^* = 4.6$ MPa, $T^* = 544$ K, $\alpha^* = 0.15$, $c^* = c_0 = 4 \times 10^5$ kg^{-1} and $We = We^*$.

The parameter profiles obtained at different v^* values are presented in figure 9. At the starting point of the wave, the Weber number reaches its critical value and bubbles begin to break up. Owing to the fragmentation, the interfacial area increases and boiling intensifies. The pressure decreases (since the bubble number n is in the numerator of (4.5)). The increase in pressure gradient $\mathrm{d}P/\mathrm{d}z$ causes an increase in the difference of phase velocities Δv (see (4.6)). The increase in Δv is why the Weber number (2.25) does not decrease after breakup in spite of the diminishing bubble radius and so breakup is repeated. Thus, it proceeds like a chain reaction, i.e. one breakup creates the conditions for the next one. That leads to a great increase in bubble number. Bubble fragmentation comes to an end when the mixture reaches an equilibrium state ($T_l = T_g$). Then, the intensity of the interphase heat exchange j approaches zero. In accordance with (2.37), $\mathrm{d}P/\mathrm{d}z \to 0$ and the chain fragmentation is switched off. As a result, 'step-like' solutions (OA, OB in figure 9) are obtained. Regimes of this type are realized if the oncoming velocity is less than a limiting value $v^* = 23.76$ m s^{-1}.

The regime OB, when the flow accelerates up to the equilibrium speed of sound a_e, is realized in the calculations with the full model, as the condition $v = a_e$ ensures the 'linkage' of the wave of boiling with the waves following it.

At $v^* > 23.76$ m s^{-1}, the flow velocity increases up to the sonic one $u = a_f$ earlier than the phases come to equilibrium. The denominator in the right part of (4.5) becomes equal to zero, the parameter gradients tend to infinity and the solutions break

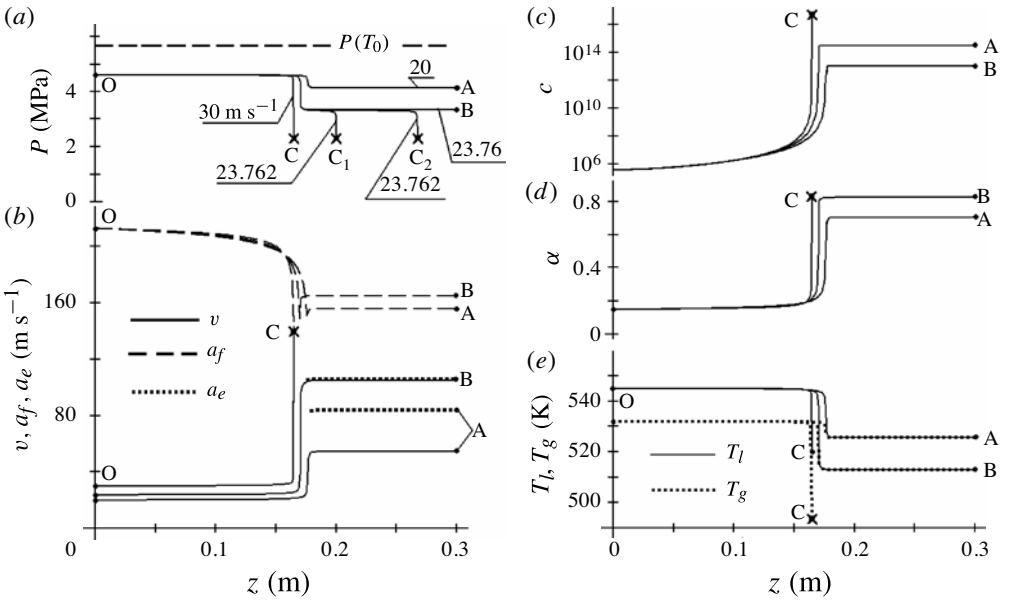

FIGURE 9. The structure of the boiling wave calculated with stationary equations (2.34)–(4.3). The curves correspond to different values of the flow velocity in front of the wave (shown in m s^{-1} in (*a*)). (*b–e*) The distribution of the other parameters along the channel for three typical regimes OA, OB and OC.

off. A series of broken-off solutions, OB_1, OB_2 and OC, obtained at $v^* > 23.76$ m s^{-1}, are shown in figure 9.

Thus, the boiling wave is formed in a flow if two conditions are fulfilled: the Weber number must reach its critical value,

$$We = We^*, \tag{4.8}$$

and the mass flux through the wave must be less than a critical value corresponding to the mass flux in regime OB,

$$g \leqslant g_B = (\rho a_e)_B\,. \tag{4.9}$$

4.2. *Calculation of stationary critical nozzle flow with the model of boiling at a constant number of centres*

Prior to passing on to the calculation of a stationary nozzle flow with the model accounting for bubble breakup, we will calculate the flow using the model of boiling at a constant number of centres. The stationary system of equations of the model with no breakup (2.14)–(2.18) is given in § 2.3.

Let us state the boundary problem: P_0 and T_0 denote the stagnation pressure and temperature at the inlet of the nozzle; varying the mass flux value, we will build the range of solutions trying to satisfy the boundary condition at the exit, $P = P_{at}$ (figure 10).

A subsonic regime OA_1 is realized at the mass flow rate $G_1 = 28.83$ kg s^{-1}. The pressure is minimal at point X_1 where the numerator (2.15) becomes equal to zero. Increasing the mass flux, we obtain the regime OA_2, which is also subsonic, but with velocity closer to the speed of sound a_f and the numerator (2.15) closer

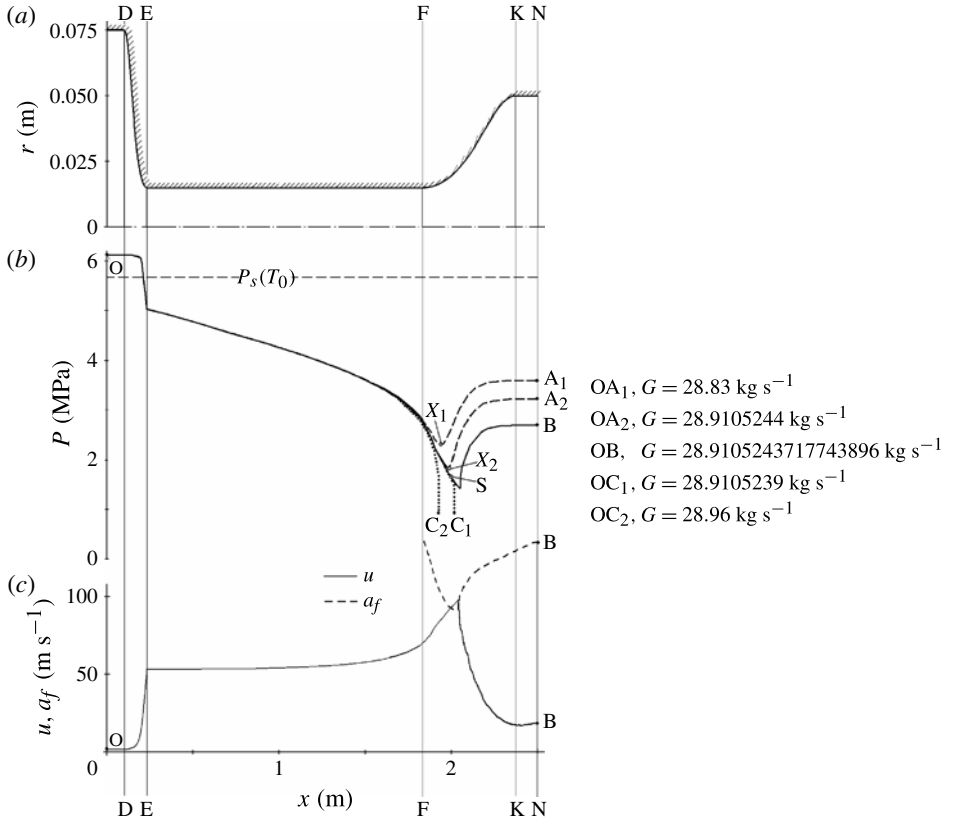

FIGURE 10. Calculation of a steady-state flow through the 'Indira' nozzle with the model of boiling at a constant number of centres. (*a*) Nozzle profile. (*b*) Pressure profiles at different values of the mass flow rate. (*c*) The distributions of the flow velocity and speed of sound in the regime OB.

to zero at the point of minimal pressure X_2. Increasing further the mass flux up to $G_{OB} = 28.910\,524\,371\,774\,3896$ kg s^{-1}, we obtain the critical regime OB with a singular point S at which the numerator and denominator of (2.15) simultaneously become equal to zero. At the singular point, the flow velocity reaches the speed of sound (see figure 10*c*). The 'supersonic zone' located between the point S and the jump of compression where the flow becomes subsonic again is rather narrow in this flux.

If the mass flux is greater than the critical one, the numerator becomes equal to zero earlier than the denominator does, the parameter gradients tend to infinity and we obtain 'broken off' solutions: regimes OC_1 and OC_2 in figure 10.

It is impossible to calculate the value of G_{OB} and obtain the regime with a singular point by means of direct integration. A detailed analysis of difficulties in 'passing' through singular points in non-equilibrium nozzle flows is given by Bilicki *et al.* (1987). We have obtained the regime OB with a singular point S shown by the solid line in figure 10 with the method of 'model expansion' described in the Appendix. (The critical regime calculated using the method of flow set-up is shown by dashed lines in figure 5, left). However, integrating system (2.14)–(2.18) directly, one can

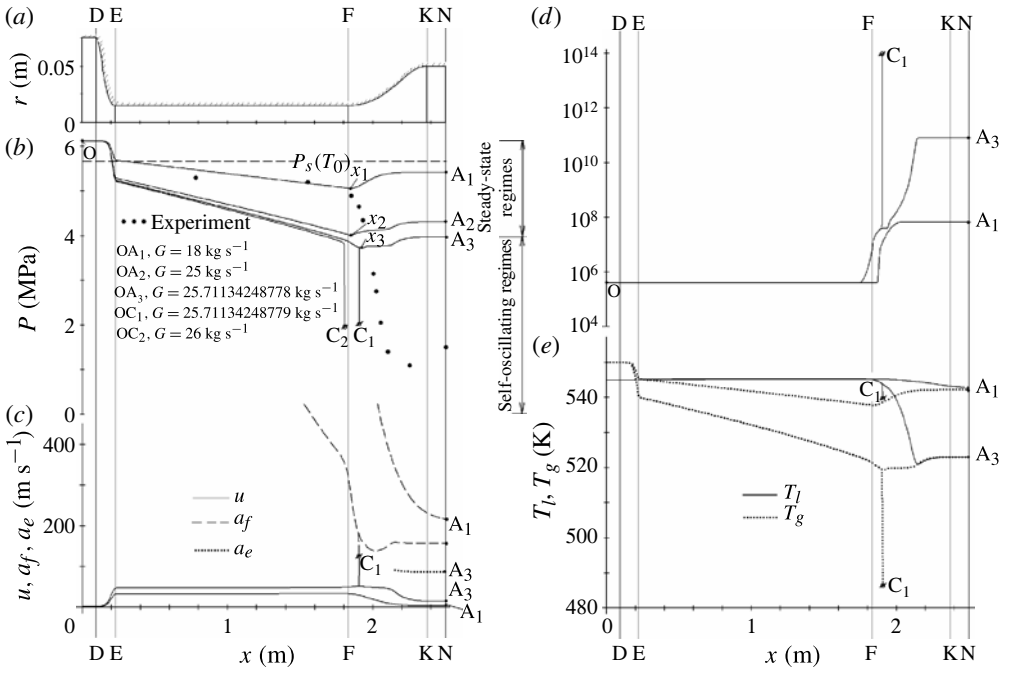

FIGURE 11. Calculation of a steady-state flow through the 'Indira' nozzle with the model accounting for bubble fragmentation. (*a*) Nozzle profile. (*b*) Experimental and calculated pressure profiles for mass flow rate 18, 25, 25.711 342 487 78, 25.711 342 487 79 and 26 kg s^{-1} (curves OA_1, OA_2, OA_3, OC_1 and OC_2, respectively. (*c–e*) The distributions of (*c*) the flow and sonic velocities, (*d*) the bubble number and (*e*) the phase temperatures in regimes OA_1, OA_3 and OC_1.

approach this point with any degree of accuracy by means of building the series of points X_i.

4.3. *Calculation of stationary critical nozzle flow with bubble breakup*

Let us now solve the problem stated in § 4.2 with the stationary analogue of the model accounting for bubble fragmentation (2.32)–(2.37). This set of equations differs from the system (4.2)–(4.7) used for the calculation of a boiling wave structure in § 4.1 in that it takes into account the change in the channel cross-sectional area and the flow wall friction. Besides, the location of the flow point where $We = We^*$ is not imposed but determined.

Finding solutions corresponding to different values of the mass flow rate G (figure 11), we are trying to approach a singular point in the same way as we did in § 4.2. The regime OA_1 obtained with mass flux $G = 18$ kg s^{-1} is a subsonic one (figure 11*c*). The point at which the numerator (2.33) is equal to zero is denoted X_1. Bubble breakup occurs in a different way from chain bubble fragmentation in a boiling wave. The term with F_x in the numerator of (2.33) is positive, $F_x > 0$, and dominating. The positivity of the numerator and the denominator ($u < a_f$) results in a positive pressure gradient (figure 11*b*) and a negative phase slip $\Delta u = u_g - u < 0$ (see (2.36)). Bubble fragmentation occurs at points where the Weber number reaches its critical value.

The fragmentation in the regime OA_1 caused by the channel geometry can be called 'coercive'. In contrast to 'chain' bubble breakup, the liquid outruns bubbles and the fragmentation is accompanied by the increase in pressure. Coercive fragmentation is not intensive: the increase in the bubble number is small (line OA_1 in figure 11*d*), and the phases do not have time to reach thermal equilibrium within the channel length (figure 11*e*).

Increasing the mass flux up to $G = 25.711\,342\,487\,78$ kg s^{-1}, we obtain a subsonic regime OA_3. At point X_3 where the numerator (2.33) is equal to zero, the denominator is rather far from zero ($M_f < 0.4$, see velocity profiles in figure 11*c*). In this regime, two 'fragmentation' sections are seen in the curve for the bubble number: the first one is at the beginning of the diffuser, and the second section is downstream (figure 11*d*). In the first section, the term with j in (2.33) responsible for interface heat exchange dominates and bubble breakup proceeds following a chain scheme. Then the 'geometry' term F_x becomes greater, the numerator (2.33) and the pressure gradient (figure 11*b*) change their signs, and bubble fragmentation is rerun following a coercive scheme.

At a negligible increase in the mass flow rate up to $25.711\,342\,487\,79$ kg s^{-1} (the change is in the 13th digit), the chain reaction no longer stops (regime OC_1). As a result, the intensity of evaporation increases by orders. The term $Q = jn(\rho_g^{-1} - \rho_l^{-1})$ in the numerator of (2.33) dominates. Chain breakup can no longer be suppressed by diffuser walls. A singular point (where the numerator and denominator are simultaneously equal to zero) cannot appear until the mixture comes to equilibrium and Q approaches zero. However, this conversion is impossible at a mass flow rate exceeding the limit value $G_{max} \approx g_{OB}F_{min} \approx 12$ kg s^{-1} (condition (4.9)). As a result, the mixture keeps being non-equilibrium (see temperature profiles in figure 11*e*), Q remains great, the denominator alone becomes equal to zero and the solution breaks off (point C_1).

Thus, there is no solution of our boundary problem having a singular point, i.e. there is no critical steady-state flow. The regimes obtained are either significantly subsonic like OA or are broken off like OC. Therefore, in accordance with the model accounting for bubble fragmentation, there is no steady-state regime of boiling liquid efflux in the 'Indira' nozzle if the back-pressure at the nozzle outlet is less than the pressure at point B, ≈4 MPa (figure 11*b*).

The following qualitative picture can help us to understand the way in which autovibrations are generated. Bubble fragmentation allows an instant conversion of a non-equilibrium boiling mixture into an equilibrium state, which is realized in a 'slow boiling wave'. The mass flux of an equilibrium mixture through the 'Indira' nozzle is $G \approx 15$ kg s^{-1} (figure 5*c*, left). At such a small flow rate, condition (4.8) for boiling wave formation cannot be realized. Vibrations increase the difference in phase velocities, and the condition for the Weber number to equal its critical value (4.8) can be fulfilled at 'small' mass fluxes 'satisfying' condition (4.9).

4.4. *Design of a nozzle that eliminates the self-oscillations*

In § 4.3, the absence of a stationary efflux through the nozzle was explained by the impossibility of boiling wave formation in a steady-state regime. To verify this conclusion, we will construct a nozzle in which a slow wave is formed at a stationary regime of efflux. We will carry out the hypothetical experiment using the set of stationary equations for the model accounting for bubble fragmentation (2.32)–(2.37).

We will change the nozzle geometry to ensure the formation of the wave at the throat outlet and the equality of the flow velocity behind the wave to the speed of

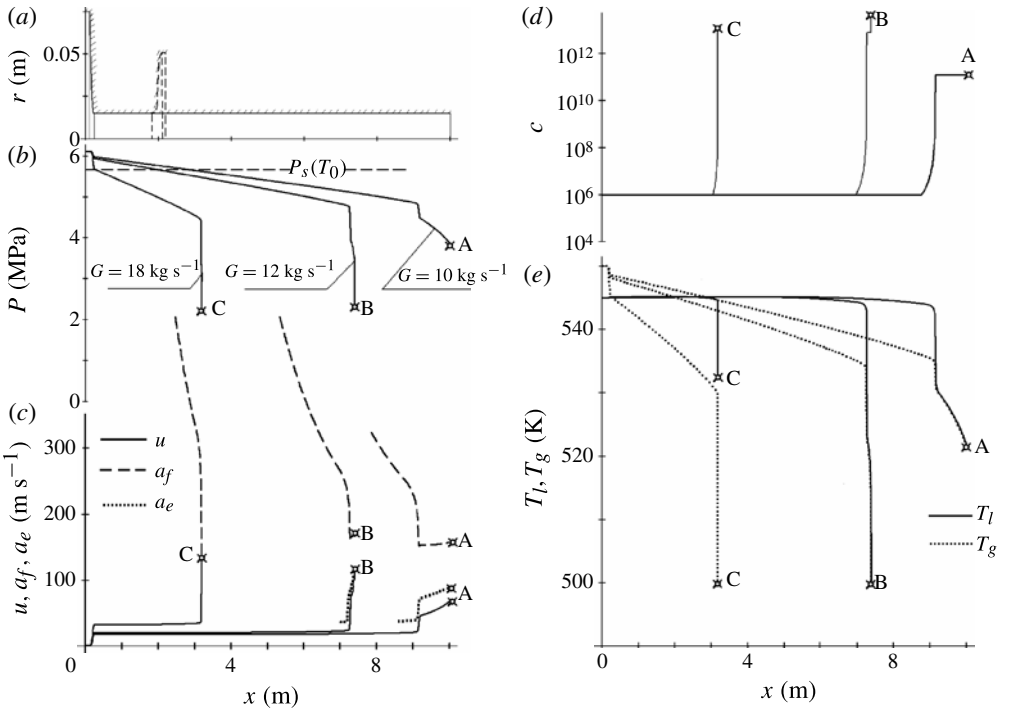

FIGURE 12. Calculation of the steady-state flow in a simplified nozzle. (*a*) Nozzle profile. (*b*) Experimental (circles) and calculated pressure profiles. (*c*) Profiles of speed of sound and flow velocity. (*d*) Bubble number. (*e*) Liquid and vapour temperatures. The mass flow rates for the regimes OA, OB, OC are 10, 12, 18 kg s^{-1}, respectively.

sound (regime OB in figure 9). In a diffuser, equilibrium flow will accelerate further, speeding up from the sonic to a supersonic velocity.

First, to terminate the position of the boiling wave, we will consider a nozzle consisting of a convergent section and a throat (figure 12*a*). The convergent section will be taken to be the same as for the 'Indira' nozzle. The profile of the origin nozzle of 'Indira' is shown by the dashed line in figure 12(*a*).

The solutions obtained with the set of stationary equations (2.32)–(2.37) for different mass fluxes are given in figure 12(*b–e*). For a mass flux close to the experimental one, $G = 18$ kg s^{-1} (regime OC), the condition $We = We^*$ is created in the section $x = 3$ m. However, this solution breaks off before the mixture comes to the equilibrium state due to the attainment of equality between the sound and the flow velocities $u = a_f$.

The flow with a boiling wave is realized at a mass flow rate 10 kg s^{-1} (regime OA). In the wave, the liquid temperature decreases to the temperature of vapour (figure 12*d*,*e*). Regime OA in figure 12 is analogous to the OA wave profile shown in figure 9. The pressure decrease behind the wave front, instead of a steady level in figure 9, is explained by the effect of the flow friction on the walls, which was not considered in the wave structure analysis (§ 4.1). Regime OA, however, is not the solution we are looking for, since the flow velocity behind the wave front is less than the speed of sound.

The regime with flow velocity equal to the equilibrium speed of sound $u = a_e$ behind the wave corresponds to a mass flow rate of 12 kg s^{-1} (regime OB). The

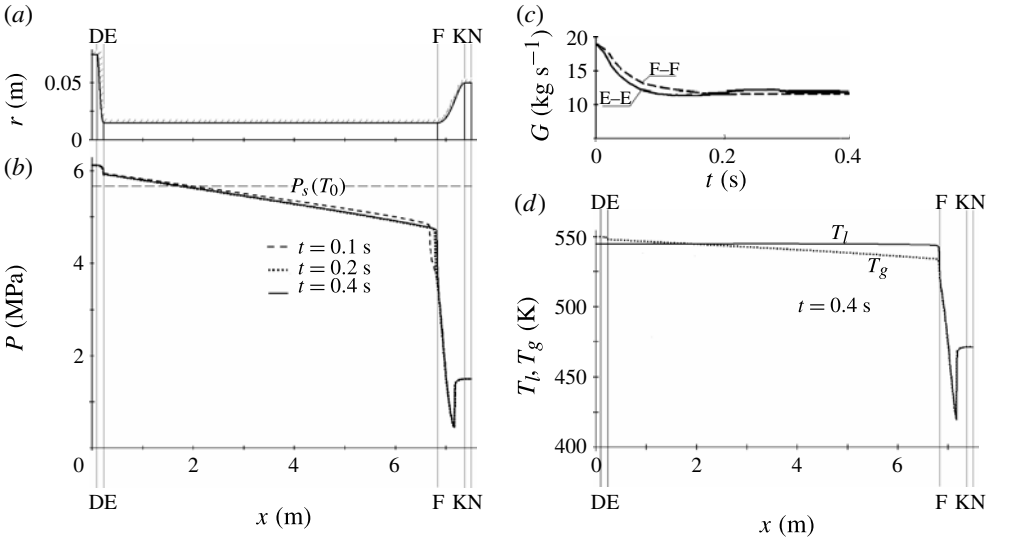

FIGURE 13. Calculation of the flow set-up in the elongated nozzle. (*a*) Nozzle profile. (*b*) Pressure profiles at instants $t = 0.1$, 0.2 and 0.4 s. (*c*) Time dependences of the mass flux at the cross-sections E–E and F–F. (*d*) Liquid and vapour temperature profiles at $t = 0.4$ s.

solution break-off downstream of the wave front is caused by the second, 'friction' term in the numerator (2.33). Owing to its presence, the numerator does not become equal to zero even in the case when the first and third (geometry and heat exchange) terms are equal to zero. Therefore the pressure gradient behind the wave tends to infinity. To avoid the solution break-off, it is necessary to replace the rectilinear section by a divergent one at the sonic point B.

Thus, for a 'boiling wave' to be stationary, the nozzle throat must be 6 m long. Now we will make the throat of the 'Indira' nozzle 5 m longer (figure 13*a*) and calculate the nozzle flow by the set-up method.

The calculations for the elongated nozzle show that, with time, the flow attains a stationary regime: the mass flux equalizes within the nozzle length (figure 13*c*). From the distributions of the phase temperatures (figure 13*d*), it is seen that the boiling wave is located near the point of the throat and diffuser junction.

Thus, the calculations using a full model have confirmed that the flow self-oscillations do not arise if the mechanism of explosive evaporation (bubble fragmentation) can be realized in a stationary flow.

5. Summary and conclusions

The predictions of the proposed model accounting for bubble fragmentation are compared with experimental data on tube and nozzle flashing flows and with models of equilibrium boiling and boiling at a constant number of centres. At the condition of no variation in free model parameters, the model taking account of bubble fragmentation has been shown to give the best predictions for flashing flows.

(*a*) The model with breakup permits an instant transition of the non-equilibrium boiling mixture into an equilibrium state due to chain bubble fragmentation taking place in boiling 'shocks'. When all the conditions for the 'shock' formation

cannot be realized in a steady-state regime, the flow goes over into a self-oscillation mode.

(*b*) The possibility of pulsations due to the periodic formation of the 'boiling waves' should be taken into account when constructing devices wherein the high mass flow rates of boiling liquid can occur.

Acknowledgement

The work was supported by the Russian Foundation for Basic Research (grant no. 12-08-162a).

Appendix. Calculation of critical nozzle flow with method of model expansion

In a critical nozzle flow, there is a point where the flow velocity becomes equal to a 'frozen' speed of sound. For the given system of (2.14)–(2.18), this critical point is somewhere in the diffuser and is a saddle one. The set of solutions in the neighbourhood of the saddle point S is shown in figure 10. There is a single solution OSB with the flow transition from subsonic to supersonic. It is impossible to obtain the separatrix OS by the method of a fourth integration of a system of ordinary differential equations (2.14)–(2.18), since it is not possible to guess the exact mass flux value G_{cr} having an infinite number of characters after the point. At a slightest deviation, the solution either turns up as the solution OA does or falls down like the solution OC does (figure 10).

A 'frozen' speed of sound

$$a_f = \left[\rho\left(\frac{(1-\alpha)\rho_l}{\beta^2} + \frac{\alpha}{P}\right)\right]^{-1/2} \tag{A 1}$$

is determined by the model assumptions. For a given model, the equality of the pressures in the liquid and vapour phases is supposed. If this assumption is 'eliminated' and the difference in phase pressures is taken into account, then the model's 'frozen' speed of sound, i.e. the velocity of propagation of high-frequency perturbations, will increase up to the speed of sound in a pure liquid, $\sim$1000 m s^{-1}. Since the flow velocity is less by an order of magnitude, the flows under consideration cannot be subsonic and do not have a critical point. The system of equations for the two-pressure model is:

$$G = \rho u F = \text{const.}, \tag{A 2}$$

$$I = i + \frac{u^2}{2} = \text{const.}, \tag{A 3}$$

$$\frac{\mathrm{d}P_l}{\mathrm{d}x} = \frac{\rho u\,\{uF_x/F - 3\alpha\omega_{la}/a - \xi|u|/(2D)\}}{1 - u^2/a_{fw}^2}, \quad F_x = \frac{\mathrm{d}F}{\mathrm{d}x}, \tag{A 4}$$

$$\frac{\mathrm{d}a}{\mathrm{d}x} = \frac{\omega_{la}}{a} + \frac{j}{4\pi a^2 \rho_l u}, \tag{A 5}$$

$$\frac{\mathrm{d}\omega_{la}}{\mathrm{d}x} = \frac{P_g - P_l}{\rho_l a u} - \frac{2\sigma - 4\mu_l\omega_{la}}{\rho_l a^2 u} - \frac{3\omega_{la}^2}{2au}, \tag{A 6}$$

$$\frac{\mathrm{d}\chi}{\mathrm{d}x} = \frac{jc}{u}, \tag{A 7}$$

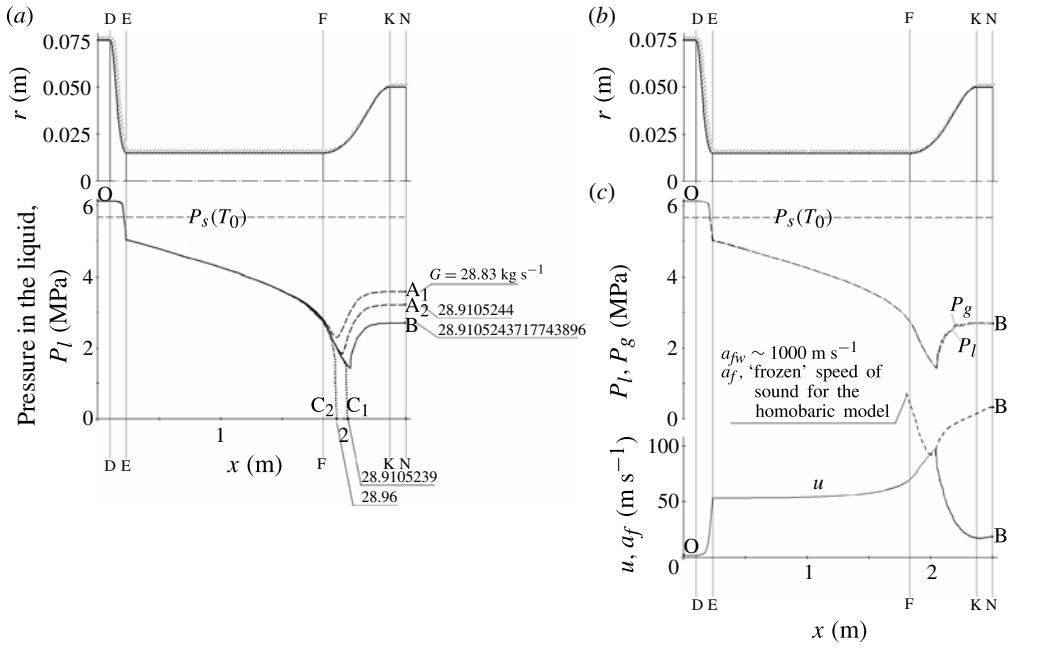

FIGURE 14. The calculation of a steady-state flow in the 'Indira' nozzle using the heterobaric model (A 2)–(A 8). (*a*) Solutions at different mass flow rates. (*b*,*c*) For the solution OB, (*b*) the pressure profiles in the liquid and vapour phases and (*c*) the flow velocity distribution. The profile of the 'frozen' speed of sound in the homobaric model calculated with (A 1) is shown in panel (*c*) by the dashed line.

$$c = \frac{n}{\rho} = \text{const.}, \tag{A 8}$$

$$a_{fw} = \frac{\beta}{\sqrt{1-\chi}}, \quad \chi = \frac{\rho_g \alpha}{\rho}, \tag{A 9}$$

where P_l and P_g are the pressures in the liquid and vapour phases; and a_{fw} is the 'frozen' speed of sound in the heterobaric model.

The boundary problem described in § 4.2 is solved. By changing the value of the mass flow rate G, we try to satisfy the boundary condition at the nozzle exit. Using a trial-and-error method, we have managed to find the solution OB that satisfies the boundary condition $P = P_{at}$ (figure 14). The profiles of P_l and P_g (figure 14*b*), the pressures in the liquid and vapour phases, are very close. Insignificant oscillations of the vapour pressure are observed around the pressure in the liquid, which are bound up with the inertia of the liquid adjoining a bubble. In figure 14(*c*) is shown the profile of the frozen speed of sound calculated on the basis of the heterobaric model using (A 1) with P_l substituted for P. In the frame of the homobaric model, the solution OB obtained is a 'supersonic' one. However, OB is subsonic in the frame of the heterobaric model (A 2)–(A 8). Instead of a single solution corresponding to the separatrix, a set of solutions with flow conversion from subsonic zone to supersonic zone (in terms of the 'homobaric' model) appears in the calculations with the heterobaric model. For these solutions, the mass fluxes are close to G_{OB} and differ in the 12th character after the point. At mass fluxes less than $G_{cr} \approx G_{OB}$, we obtain

'subsonic', in the frame of the homobaric model, solutions OA_1 and OA_2. At greater mass fluxes, we get solutions OC_1 and OC_2 with the liquid pressure decreasing below zero.

All the solutions obtained in the frame of the heterobaric model are continuous. The jumps in solutions obtained in calculations with the homobaric model have a finite width in the frame of the heterobaric model.

It should be noted that the solution OB coincides with the solution obtained by the method of flow set-up (dotted line in figure 5*b*, left).

REFERENCES

BAUER, E., HOUDAUER, G. & SUREAU, H. 1977 Interprétation des essays Moby-Dick à l'aide de modèles prenant en compte les déséquilibres thermodynamiques. European Two Phase Flow Group Meeting, Grenoble.

BILICKI, Z., DAFERMOS, C., KESTIN, J., MAJDA, G. & ZENG, D. L. 1987 Trajectories and singular points in steady-state models of two-phase flows. *Intl J. Multiphase Flow* **13** (4), 511–533.

BIRKHOFF, G. 1960 *Hydrodynamics*. Princeton University Press.

BOIVIN, J. Y. 1979 Two-phase critical flow in long nozzles. *Nucl. Technol.* **46** (3), 540–545.

DREW, D. A. & PASSMAN, S. L. 1998 *Theory of Multicomponent Fluids*. Springer.

EDWARDS, A. R. & O'BRIEN, T. P. 1970 Studies on phenomena connected with the depressurization of water reactors. *J. Br. Nucl. Engng Soc.* **9**, 125–135.

GIOT, M. 1981 Critical flows. In *Thermohydraulics of two-phase systems for industrial design and nuclear engineering* (ed. J. M. Delhaye, M. Giot & M. L. Reithmuller), pp. 405–452. Hemisphere.

HENRY, R. E. 1968 A study of one- and two-component, two-phase critical flows at low qualities. *Report* ANL-7430.

ISAEV, O. A. 1980 Liquid boiling under a fast pressure fall in an adiabatic unsteady stream. Doctor's thesis, Sverdlovsk.

ISBIN, H. S. 1980 Some observation on the status of two-phase critical flow models. *Intl J. Multiphase Flow* **6**, 131–137.

ISHII, M. & HIBIKI, T. 2006 *Thermo-Fluid Dynamics of Two-Phase Flow*. Springer.

IVANDAEV, A. I. & GUBAIDULLIN, A. A. 1978 The investigation of an unsteady efflux of boiling liquid in a thermodynamically equilibrium approximation. *Teplofiz. Vys. Temp.* **16** (3), 556–562 (in Russian).

IVASHNYOV, O. E., IVASHNEVA, M. N. & SMIRNOV, N. N. 2000 Slow waves of boiling under hot water depressurization. *J. Fluid Mech.* **413**, 149–180.

IVASHNYOV, O. E. & SOPLENKOV, K. I. 1992 A model involving break-up to explain peculiarities of boiling liquid efflux process. *Intl J. Multiphase Flow* **18** (5), 727–738.

LABUNTSOV, D. A. & AVDEEV, A. A. 1981 Theory of boiling discontinuity. *Teplofiz. Vys. Temp.* **19** (3), 552–556 (in Russian).

LABUNTSOV, D. A. & AVDEEV, A. A. 1982 The mechanism of flow choking at impact boiling of liquid. *Teplofiz. Vys. Temp.* **20** (1), 88–96 (in Russian).

LAMB, G. 1957 *Hydrodynamics*. Cambridge University Press.

LIENHARD, J. H., ALANGIR, M. & TRELA, M. 1978 Early response of hot water to sudden release from high pressure. *Trans. ASME: J. Heat Transfer* **100** (3), 473–479.

NIGMATULIN, R. I. 1991 *Dynamics of Multiphase Media*, Vols I, II. Hemisphere.

NIGMATULIN, R. I. & SOPLENKOV, K. I. 1980 The study of an unsteady efflux of boiling liquid from channels in the thermodynamically non-equilibrium approximation. *Teplofiz. Vys. Temp.* **18** (1), 118–131 (in Russian).

SCRIVEN, L. E. 1959 On the dynamics of phase growth. *Chem. Engng Sci.* **10** (1–2), 1–13.

SIVUCHIN, D. V. 1979 *The Course of Fundamental Physics. Thermodynamics and Molecular Physics*. Nauka (in Russian).

SKOREK, T. & PAPADIMITRIOU, P. 1997 A simple model for critical flashing flows in nozzles: development and experimental verification. In *Experimental Heat Transfer, Fluid Mechanics and Thermodynamics 1997* (ed. M. Giot, F. Mayinger & G.P. Celata), pp. 1701–1708. Edizioni ETS.

VAISMAN, M. L. 1967 *Thermodynamics of Vapor–Liquid Flows*. Energiya (in Russian).

WINTERS, W. S. JR & MERTE, H. JR 1979 Experiments and nonequilibrium analysis of pipe blowdown. *Nucl. Sci. Engng* **69** (3), 411–429.